

Figure 5.1. The wanted capabilities of a virtual wave flume.

It was chosen to use an already assembled SPH program SPHysics instead of building a new one because SPHysics contained all the necessary tools to model a virtual wave flume. Apart from the necessary tools to solve CFD SPH problems in 2-D and 3-D it also contained subroutines to handle geometry generation, paddle movement, obstacles in the flume and a selection of filters to help improve the solution. The theory and program structure utilized in SPHysics is described in greater detail in Section 5.1 and 5.2.

5.1 SPHysics

The program SPHysics v1.0 was released in August 2007 made jointly by the researchers at a number of universities. SPHysics is written specifically to solve free surface fluid problems using the SPH method. SPHysics is written entirely in Fortran 77 and the post processing is done with MatLab. The program is able to handle a number of different situations in two (2-D) and three (3-D) dimensions most notable the simulation of a wave flume with two different kinds of paddles. More information about the SPHysics project and the group of researchers in the SPHERic group backing it is available at [SPHysics; 2007] and [SPHERics; 2007 a&b]. Other open source SPH programs are available like the one offered by [Liu; 2003] and while it is well-arranged and more developed in terms of parallel programming it is first and foremost a demonstration tool and lacks among other things the advanced wave flume abilities. The SPHysics source code for geometry generation and the numerical solution is available for download together with its documentation [Gesteira et al; 2007].

The original version of SPHysics v1.0 is written in Fortran 77 and will henceforth be referred to as SPHysics F77. Only in and output variables are defined in F77 and the file structure made the code impractical to work with. In order to obtain an understanding off how an advanced SPH program function and learn how to work with Fortran it was decided to upgrade the existing code to Fortran 95. This new

version of SPHysics will henceforth be known as SPHysics F95 and is used for all the numerical simulations presented in this report. In this project all the work was done on the 2-D version but it is a simple matter to perform the same work on the files for 3-D computations. Any reference to SPHysics in this report is always to the 2-D version. An analysis of SPHysics F77 and a description of the applied changes are available in Appendix B.3 together with information about changes and found bugs. The following pages contain a short description of the capabilities of the code and the used theory.

Further reading about the original SPHysics source code is available in [Gesteira et al; 2007]. The source code of SPHysics F95 is available on the CD-Rom. A good place to start would be the file *Parameters.f90* where most of the variables are defined and *SPHysicsF95.f90* is the file controlling the main loop. A full flow diagram of how the subroutines interact in SPHysics and SPHysicsgen is available in the Appendix B.6.

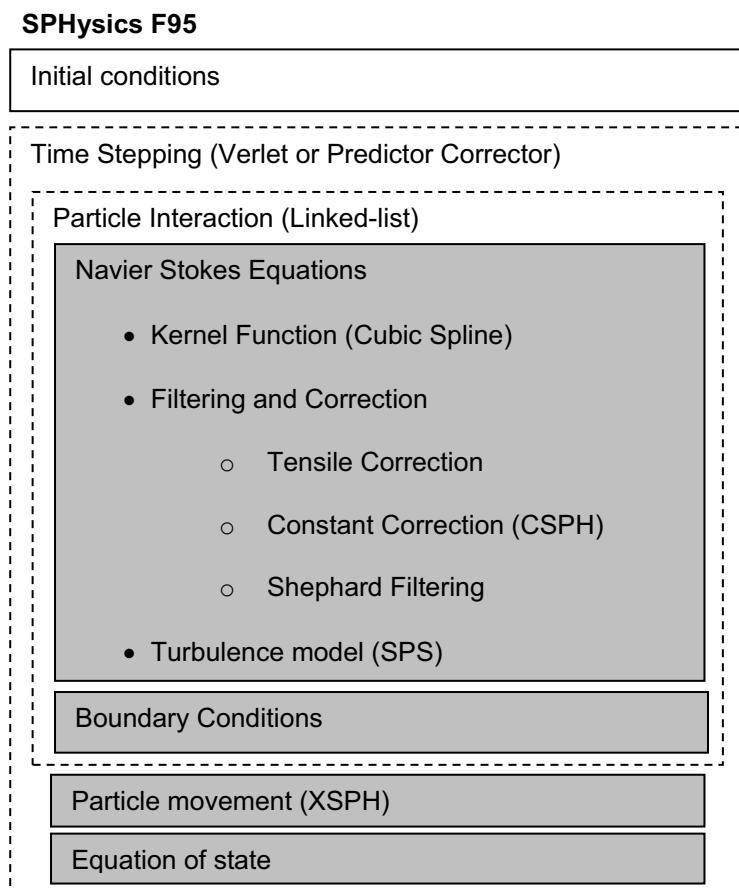


Figure 5.2. The SPHysics toolbox used in this project the different methods are introduced in the following section.

5.2 Theory - SPH with CFD

During the past 15 years the SPH method has undergone a great deal of change when it comes to solving fluid dynamics problems. Although the original SPH formulation remains the same a number of correction filters, boundary types and diffusion models have been added to improve the method. SPHysics uses a chosen combination of these methods and one of the reasons to use SPHysics for modeling instead of building a program from scratch was the possibility to get a toolbox that was already fully assembled and tested. The theory behind this toolbox is presented on the next few pages with emphasis on the methods used to build the virtual wave flume and why the method was chosen. The described methods and how they relate to each other is depicted in Figure 5.2.

The biggest difference from the SPH theory discussed in Chapter 3 is that the particles are no longer fixed in space and this makes it necessary to discuss the consistency of SPH and how it is implemented, Section 5.2.1 and 5.2.5. The particle distribution is no longer regular and the support domain might be truncated by boundaries, Figure 5.3. This is also taken into consideration when the governing Navier-Stokes equations are derived in order to limit the impact of the irregular distribution.

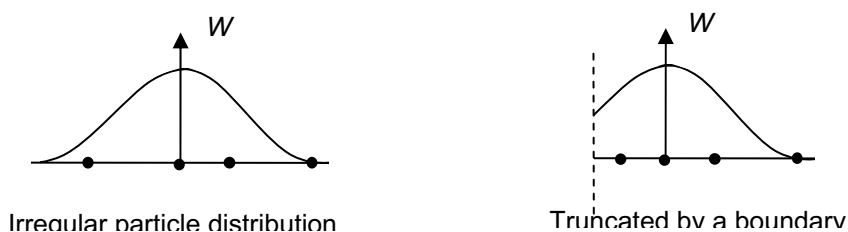


Figure 5.3. Example of how the distribution of particles beneath a kernel function and how the kernel function might be truncated by a boundary. Both situations will lead to particle inconsistency.

5.2.1 Particle inconsistency

If a numerical method is to converge it must have a certain degree of consistency. The level of consistency is measured by the degree of polynomial the chosen shape function/kernel function is able to reproduce. This term is also known as completeness in FEM and SPH has borrowed the definition of the necessary level of completeness from here. For the SPH method the necessary consistency of the kernel approximation is given in (5.1) and (5.2). They ensure that linear functions are perfectly interpolated and their gradients are exactly obtained.

$$\int_{\Omega} W(\mathbf{x} - \mathbf{x}', h) d\mathbf{x}' = 1 \quad (5.1)$$

$$\int_{\Omega} (\mathbf{x} - \mathbf{x}') W(\mathbf{x} - \mathbf{x}', h) d\mathbf{x}' = 0 \quad (5.2)$$

This leads to the consistency of the particle approximation as equation (5.1) and (5.2) does not necessarily have consistency in their discrete form (5.3) and (5.4)

$$\sum_{j=1}^N W(\mathbf{x} - \mathbf{x}_j, h) \Delta \mathbf{x}_j = 1 \quad (5.3)$$

$$\sum_{j=1}^N (\mathbf{x} - \mathbf{x}_j) W(\mathbf{x} - \mathbf{x}_j, h) \Delta \mathbf{x}_j = 0 \quad (5.4)$$

The discretized consistency conditions given as (5.3) and (5.4) are easily brought out of balance if the support domain is truncated or if the particle distribution in the support domain is unbalanced, Figure 5.3. This is a problem called particle inconsistency when working with moving particles and is solved in SPHysics F95 by using a normalization scheme (CSPH) described in Section 5.2.5. [Liu; 2003]

5.2.2 Smoothing length

The smoothing length h is chosen as a constant in SPHysics defined by equation (5.5). Where dx and dz is the initial particle spacing and k_h is a coefficient chosen as 0.92 in 2-D no matter what kernel is used in order to create a support domain covering the neighbouring particles.

$$h = k_h \cdot \sqrt{dx^2 + dz^2} \quad (5.5)$$

From Section 3.4 it is known that the smoothing length has an impact on the quality of the solution. When the particles in 2-D are moving is the optimal h of course hard to predict. [Liu; 2003] introduce the possibility of a variable smoothing length in order to optimize the solution. This possibility is not available in SPHysics F95 and will not be discussed further in this report. Furthermore will the CSPH normalization limit the disadvantages of a constant h as it correct the kernel to the current particle distribution in order to fulfil the consistency. The constant h should approximate the average particle distance throughout the solution.

5.2.3 Kernel functions

Two new kernels are available in SPHysics F95 together with the Gaussian and the Cubic Spline kernel, Table 3.1. The new kernel functions must fulfil the same conditions as the other kernel functions described in Section 3.3 and are presented in Table 3.1. All kernel functions in SPHysics have a κ equal to four;

Table 5.1. List of kernel functions available in SPHysics for 2 and 3-D [Gesteira et al; 2007] and [Wendland; 1995]

Kernel name	Equation	Eq. no
Quadratic	$W(R, h) = \alpha_d \left(\frac{3}{16} R^2 - \frac{3}{4} R + \frac{3}{4} \right) \quad 0 \leq R \leq 2$	(5.6)
Wendland	$W(R, h) = \alpha_d \left(1 - \frac{R}{2} \right)^4 (2R + 1) \quad 0 \leq R \leq 2$	(5.7)

Table 5.2. List of the constant α_d used together with kernel functions in Table 3.1

Kernel name	Eq. no.	κ	2-D (α_d)	3-D (α_d)
Quadratic	(5.6)	4	$1/(\pi h^2)$	$1/(\pi h^3)$
Wendland	(5.7)	4	$7/(4\pi h^2)$	$7/(8\pi h^3)$

5.2.4 Navier-Stokes Equations

The Navier-Stokes equations for a Newtonian compressible fluid are the governing equations when modeling fluid dynamics in SPHysics. The Newtonian fluid has a linear relationship deformation and tension. It is necessary to define the fluid as compressible rather than the common incompressible approach to allow the use of an Equation of state and thereby speed up the computation, Section 5.2.7. The governing equations are following the three laws of conservation.

- Conservation of mass ensured by the continuity equation
- Conservation of momentum ensured by the momentum equation
- Conservation of energy ensured by the energy equation

The three equations are derived on the following pages and transferred to the SPH formulation used in SPHysics finally presented in Box 5.1. The equations are derived with regard to the total derivative D/Dt i.e. the derivative is following the motion of the fluid defined in (5.8) as a sum of the local and the convective derivative where v is the speed.

$$\frac{D}{dt} = \frac{\partial}{\partial t} + \frac{\partial}{\partial x^\alpha} v^\alpha \quad (5.8)$$

In other SPH literature the derivative follow the motion defined as d/dt defined in [Monaghan; 1992]. This section is written based on [Liu; 2003] & [Brorsen; 2005] and will use an index notation where α and β placed as superscripts is used to denote the coordinate directions (2D: $\alpha, \beta = 1, 2$ and 3D: $\alpha, \beta = 1, 2, 3$). This is demonstrated by writing the definition of Kronecker's tensor in equation (5.9).

$$\delta^{\alpha\beta} = \begin{cases} 1 & \text{if } \alpha = \beta \\ 0 & \text{if } \alpha \neq \beta \end{cases} \quad (5.9)$$

Furthermore it is necessary to make a few definitions with regard to the definition of strain and stress. The connection between shear stress $\tau^{\alpha\beta}$ and the viscous shear strain rate $\varepsilon^{\alpha\beta}$ is defined by equation (5.10) where μ_d is the dynamic viscosity. The equation is in the literature known as *Newton's equation* and has been experimentally validated.

$$\tau^{\alpha\beta} = 2\mu\varepsilon^{\alpha\beta} \quad (5.10)$$

The total stress tensor is defined as the sum of the shear stress and the isotropic pressure (5.11).

$$\sigma^{\alpha\beta} = -p\delta^{\alpha\beta} + \tau^{\alpha\beta} \quad (5.11)$$

$$\varepsilon^{\alpha\beta} = \frac{1}{2} \left(\frac{\partial v^\beta}{\partial x^\alpha} + \frac{\partial v^\alpha}{\partial x^\beta} \right) - \frac{1}{3} v^{\lambda,\lambda} \delta^{\alpha\beta} \quad (5.12)$$

The shear strain rate $\varepsilon^{\alpha\beta}$ is defined for a compressible Newtonian fluid in (5.12). The shear strain rate consists of two parts representing the deformation velocity tensor and dilatation. In case of an incompressible fluid the dilatation part will be equal to zero. Instead of μ_d it is possible to use the kinematic viscosity μ_K defined in equation (5.13). The kinematic viscosity is an input in SPHysics.

$$\mu_k = \frac{\mu_d}{\rho} \quad (5.13)$$

The stress vector \mathbf{t} on a arbitrary surface ΔA in the fluid is defined by the normal \mathbf{n} on the surface and the force ΔF defined in (5.14).

$$\left(\frac{\Delta F^\alpha}{\Delta A} \right)_{\Delta A \rightarrow 0} = \frac{dF^\alpha}{dA} = \mathbf{t}^\alpha \quad (5.14)$$

5.2. Theory - SPH with CFD

Using this definition it is possible to define the relation between the stress vector and the total stress tensor $\sigma^{\alpha\beta}$ for a fluid (5.15). The definition is used when deriving the momentum equation.

$$\sigma_N^\alpha = \sigma^{\alpha\beta} n^\alpha \quad (5.15)$$

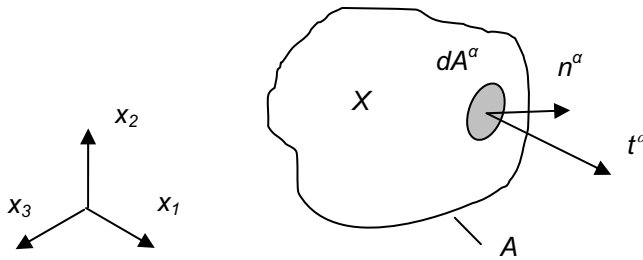


Figure 5.4. The body and surface forces on a volume X with the area A . This arbitrary volume is used to derive a continuity and momentum.

The divergence theorem (5.16) is presented as it is used to derive Navier-Stokes equations.

$$\int_A (\mathbf{F} \cdot \mathbf{n}) dA = \int_V (\nabla \cdot \mathbf{F}) dV \quad (5.16)$$

Continuity equation (Conservation of mass)

The method to conserve mass is important in the SPH method as the mass is used to calculate the density using the equation of density approximation from Box 5.1. Presented here as equation (5.17).

$$\rho_i = \sum_{j=1}^J m_j W_{ij} \quad (5.17)$$

It would of course be possible to use (5.17) directly to conserve the mass as m_i is a constant i.e. the mass would be conserved as long as the number of particles J is the same. However, using this equation directly is not possible when modelling a free surface as the density would decrease close to interfaces like fixed boundaries or free surfaces [Monaghan; 1992]. Instead it is necessary to derive a second method based on the continuity equation.

The continuity equation states the constancy of mass in the current of a continuum. It is found by looking at flux through an arbitrary area A that serves as the surface of the volume X . The growth in mass inside A is equal to the mass that flows through A each time unit leading to equation (5.18).

$$\int_X \frac{\partial \rho}{\partial t} dX = \int_A -\rho v^\alpha dA^\alpha \quad (5.18)$$

$$dA^\alpha = n^\alpha dA \quad (5.19)$$

where

dA is part of the area A [m^2]

ρ is the density [kg/m^3]

Rewriting this is possible by using the divergence theorem (5.20) together with (5.18) leading to equation (5.21).

$$\int_A (-\rho v^\alpha) dA^\alpha = - \int_X \frac{\partial (\rho v^\alpha)}{\partial x^\alpha} dX \quad (5.20)$$

$$\int_X \frac{\partial \rho}{\partial t} dX = - \int_X \frac{\partial (\rho v^\alpha)}{\partial x^\alpha} dX \Rightarrow \int_X \left(\frac{\partial \rho}{\partial t} + \frac{\partial (\rho v^\alpha)}{\partial x^\alpha} \right) dX = 0 \quad (5.21)$$

This equation must be valid for any choice of X allowing the following rewriting to the finished continuity equation written as a global derivative in index (5.22) and vector notation (5.23).

$$\frac{D\rho}{dt} + \rho \frac{\partial v^\alpha}{\partial x^\alpha} = 0 \quad (5.22)$$

$$\frac{D\rho}{Dt} = -\rho \nabla \cdot \mathbf{v} \quad (5.23)$$

There are two different approaches to conserve the mass in SPH. One approach has already been presented in equation (5.17) and it is now possible to derive a second SPH formulation using (5.22) as a base together with SPH approximation of Box 5.1. The equation (5.22) is rewritten using the following identity.

$$-\rho \frac{\partial v^\beta}{\partial x^\beta} = - \left(\frac{\partial \rho v^\beta}{\partial x^\beta} - \frac{\partial \rho}{\partial x^\beta} v^\beta \right) \quad (5.24)$$

$$\frac{D\rho}{dt} = -\rho \frac{\partial v^\alpha}{\partial x^\alpha} = -\left(\frac{D\rho v^\beta}{dx^\beta} - v^\beta \frac{D\rho}{dx^\beta} \right) \quad (5.25)$$

The equation is now rewritten in equation (5.26)-(5.29) using SPH approximation.

$$\frac{D\rho_i}{dt} = -\left[\sum_{j=1}^N \frac{m_j}{\rho_j} (\rho_j v_j^\beta) \frac{\partial W_{ij}}{\partial x_i^\beta} - v_i^\beta \left(\sum_{j=1}^N \frac{m_j}{\rho_j} (\rho_j) \frac{\partial W_{ij}}{\partial x_i^\beta} \right) \right] \quad (5.26)$$

$$\frac{D\rho_i}{dt} = -\sum_{j=1}^N m_j v_j^\beta \cdot \frac{\partial W_{ij}}{\partial x_i^\beta} + \sum_{j=1}^N m_j v_i^\beta \frac{\partial W_{ij}}{\partial x_i^\beta} \quad (5.27)$$

$$\frac{D\rho_i}{dt} = \sum_{j=1}^N m_j (v_i^\beta - v_j^\beta) \frac{\partial W_{ij}}{\partial x_i^\beta} \quad (5.28)$$

The final approximation is written in vector notation with $\mathbf{v}_{ij} = (v_i^\beta - v_j^\beta)$.

$$\frac{D\rho_i}{Dt} = \sum_{j=1}^N m_j \mathbf{v}_{ij} \cdot \nabla_i W_{ij} \quad (5.29)$$

The final equation (5.29) is commonly used for density approximation with the SPH method presented first by [Monaghan; 1992]. When using this approximation the density of all particles defined initially and the change in density are closely related to the neighbouring particles in the support domain. It is not the only possible way to derive a particle approximation of the Continuity equation but it is used due to several inherent advantages. Firstly, \mathbf{v}_{ij} accounts for the relative velocity of a particle pair in the support domain and it helps to reduce errors from particle inconsistency, i.e. an uneven distribution of the particles.

The two different ways to conserve mass are the summation density approach (5.17) and continuity density approach (5.29). The density approach conserves mass the exactly continuity approach does not. It does however not have the same problems at the boundaries and the fluid surface. Furthermore when approximating between the particles it is necessary to do the approximation twice when using (5.17). The continuity approach is used in SPHysics together with a Shephard filtering discussed in Section 5.2.5 to speed up calculation. [Liu; 2003]

Constitutive equation

The Constitutive equation is not one of the three conservation equations but it is nonetheless important as it defines the relationship between the total stress tensor $\sigma^{\alpha\beta}$ and the deformation. Experiments show that water has linear relation between stress and deformation defining it as a Newtonian fluid with the constitutive equation (5.30) for a fluid in motion.

$$\sigma^{\alpha\beta} = -p\delta^{\alpha\beta} + \tau^{\alpha\beta} = -p\delta^{\alpha\beta} + 2\mu\varepsilon^{\alpha\beta} \quad (5.30)$$

$$p = -\frac{1}{3}(\sigma^{11} + \sigma^{22} + \sigma^{33}) \quad (5.31)$$

The pressure p is defined as (5.31) in a moving fluid. It is possible to assume isotropic pressure as it may be shown that the motion of the fluid only will cause a small deviation from this distribution of pressure. [Brorsen; 2005]

Momentum equation (Conservation of momentum)

The momentum equation is derived for a Newtonian fluid and the conservation of momentum is assured by using Newton's second law as the net force on a volume X consist of the body forces and surface forces.

The gravitational force $F_g = \rho\mathbf{g}$ and the inertia force $(-D\mathbf{v}/Dt)$ are the body forces in SPHysics defined in equation (5.32) where b^α is the sum of body forces.

$$b^\alpha = g^\alpha - \frac{Dv^\alpha}{Dt} \quad (5.32)$$

The surface forces are found with the help of the stress vector \mathbf{t} defined in equation (5.15). This leads to equation (5.33) as the net force on the volume is equal to zero.

$$\int_A \mathbf{t}^\alpha dA + \int_X \rho b^\alpha dX = 0 \quad (5.33)$$

Using the divergence theorem and the definition of \mathbf{t} it is possible to rewrite equation (5.33).

$$\int_A \mathbf{t}^\alpha dA = \int_X \frac{\partial \sigma^{\alpha\beta}}{\partial x^\beta} dX \quad (5.34)$$

$$\int_X \left(\frac{\partial \sigma^{\alpha\beta}}{\partial x^\beta} + \rho b^\alpha \right) dX = 0 \quad (5.35)$$

Reasoning that this equation must be true for an arbitrary volume X equation (5.36). The body force equation is substituted into the finished momentum equation (5.37) for a fluid.

$$\frac{\partial \sigma^{\alpha\beta}}{\partial x^\beta} + \rho b^\alpha = 0 \quad (5.36)$$

$$\frac{Dv^\alpha}{Dt} = \frac{1}{\rho} \frac{\partial \sigma^{\alpha\beta}}{\partial x^\beta} + g^\alpha \quad (5.37)$$

The momentum equation (5.37) is now rewritten using the identity (5.38) to prepare for SPH approximation of the derivatives. This use of this identity and how it is used to reach a particle approximation is derived in Appendix A.

$$\frac{1}{\rho} \frac{\partial \sigma^{\alpha\beta}}{\partial x^\beta} = \frac{\partial}{\partial x^\beta} \left(\frac{\sigma^{\alpha\beta}}{\rho} \right) + \frac{\sigma^{\alpha\beta}}{\rho^2} \frac{\partial \rho}{\partial x^\beta} \quad (5.38)$$

$$\frac{Dv^\alpha}{Dt} = \frac{\partial}{\partial x^\beta} \left(\frac{\sigma^{\alpha\beta}}{\rho} \right) + \frac{\sigma^{\alpha\beta}}{\rho^2} \frac{\partial \rho}{\partial x^\beta} + g^\alpha \quad (5.39)$$

Following a particle approximation and rearranging of the equation it is possible to write equation (5.40) as an SPH formulation of the momentum equation. The identifier was used to add symmetry to the final equation reducing the error from particle inconsistency.

$$\frac{Dv_i^\alpha}{Dt} = \sum_{j=1}^J m_j \left(\frac{\sigma_i^{\alpha\beta}}{\rho_i^2} + \frac{\sigma_j^{\alpha\beta}}{\rho_j^2} \right) \frac{\partial W_{ij}}{\partial x_i^\beta} + g^\alpha \quad (5.40)$$

The viscous shear stress and the isotropic pressure is separated and a new variable Ψ_{ij} representing the viscosity is defined as (5.42) where ε is the strain rate and μ is the dynamic viscosity in a Newtonian fluid

$$\frac{Dv_i^\alpha}{Dt} = \sum_{j=1}^J m_j \left(-\frac{P_i}{\rho_i^2} - \frac{P_j}{\rho_j^2} + \left(\frac{\tau_i^{\alpha\beta}}{\rho_i^2} + \frac{\tau_j^{\alpha\beta}}{\rho_j^2} \right) \right) \nabla_i W_{ij} + g^\alpha \quad (5.41)$$

$$\Psi_{ij}^{\alpha\beta} = \left(\frac{\tau_i^{\alpha\beta}}{\rho_i^2} + \frac{\tau_j^{\alpha\beta}}{\rho_j^2} \right) \quad (5.42)$$

Finally the momentum equation is written in vector notation as (5.43).

$$\frac{D\mathbf{v}_i}{Dt} = -\sum_{j=1}^J m_j \left(\frac{P_i}{\rho_i^2} + \frac{P_j}{\rho_j^2} \right) \nabla_i W_{ij} + \sum_{j=1}^J m_j \boldsymbol{\psi}_{ij} \nabla_i W_{ij} + \mathbf{g} \quad (5.43)$$

This version of the momentum equation is used commonly in SPH codes and in SPHysics. The viscosity term is solved either by using an artificial viscosity or a turbulence model presented in 5.2.6. [Liu; 2003]

Energy equation (Conservation of energy)

The conservation of energy is based on the first law of thermodynamics where the change in internal energy is equal to the heat added to the system minus the conducted work. As there is no heat added to the system in the SPH formulation the only source of change of internal energy in the infinitesimal fluid cell consists of the work done by the body forces. The work done by the body forces consist of the isotropic pressure multiplying the volumetric strain and the energy dissipation due to the viscous shear forces. It follows that the heat equation is (5.44) where $\sigma^{\alpha\beta}$ is the total stress tensor defined in equation (5.11).

$$\frac{De}{dt} = \frac{\sigma^{\alpha\beta}}{\rho} \frac{\partial v^\alpha}{\partial x^\beta} \quad (5.44)$$

SPH approximation in SPHysics is taken from [Monaghan; 1994] who presents the equation (5.45) where Ψ is the viscosity terms which are calculated using artificial viscosity or SPS viscosity, Section 5.2.6.

$$\frac{De_i}{dt} = \frac{1}{2} \sum_{j=1}^J m_j \left(\frac{P_i}{\rho_i^2} + \frac{P_j}{\rho_j^2} + \boldsymbol{\psi}_{ij} \right) v_{ij} \nabla_i W_{ij} \quad (5.45)$$

Several alternatives to this equation are given in [Liu; 2003] but it is also stated that there is no noticeable difference between them.

Box 5.1. SPH equations for the Navier-Stokes equations

Conservation of mass

$$\frac{D\rho_i}{Dt} = \sum_{j=1}^N m_j \mathbf{v}_{ij} \cdot \nabla_i W_{ij} \quad (5.29)$$

Conservation of momentum

$$\frac{Dv_i^\alpha}{Dt} = \sum_{j=1}^J m_j \left(\frac{\sigma_i^{\alpha\beta}}{\rho_i^2} + \frac{\sigma_j^{\alpha\beta}}{\rho_j^2} \right) \nabla_i W_{ij} + g^\alpha \quad (5.41)$$

$$\frac{Dv_i}{Dt} = \sum_{j=1}^J m_j \left(\frac{P_i}{\rho_i^2} + \frac{P_j}{\rho_j^2} + \psi_{ij} \right) \nabla_i W_{ij} + \mathbf{g} \quad (5.43)$$

Conservation of energy

$$\frac{De_i}{dt} = \frac{1}{2} \sum_{j=1}^J m_j \left(\frac{P_i}{\rho_i^2} + \frac{P_j}{\rho_j^2} + \psi_{ij} \right) \mathbf{v}_{ij} \cdot \nabla_i W_{ij} \quad (5.45)$$

5.2.5 Correction and filters

The following is three methods used to enhance and stabilize the solutions generated with the SPH method. They have all been developed to help when solving fluid problems during the last decade. The XSPH correction that moves the particles and is described separately in Section 5.2.9 is the last member of the group.

CSPH correction

The corrected SPH interpolation is conducted to ensure that the consistency equations (5.1) and (5.2) is satisfied exactly after the particle approximation (5.3) and (5.4). The scope is to introduce an adjusting factor presented in equation (5.46) to produce a corrected kernel [Kulasegaram & Bonet; 2000]

$$\widehat{W}_i(\mathbf{x}) = W_i(\mathbf{x}) \alpha(\mathbf{x}) [1 + \boldsymbol{\beta}(\mathbf{x}) \cdot (\mathbf{x} - \mathbf{x}_b)] \quad (5.46)$$

The correction parameters $\alpha(\mathbf{x})$ and $\beta(\mathbf{x})$ enforces the consistency of the particle approximation by deriving them from (5.3) and (5.4) using simple substitution with (5.46). This is not the scope of this report but the derived equations enable an explicit evaluation of the parameters and ensure that the linear functions and their gradients are exactly obtained.

The CSPH approach (also known as an RKPM: Reproducing Kernel Particle Method) is one of two ways to ensure consistency the other is described by [Liu; 2003].

Shephard filtering

Shephard filtering is performed to ensure that the free surface is smooth and physically acceptable. The filter is necessary when using LES to model the viscous forces as density variations are being magnified by the equation of state, Section 5.2.7. The filter is not necessary with artificial viscosity from [Monaghan; 1992] as it damps out the variations. In SPHysics F95 the filtering is performed every 30 time steps. [Dalrymple and Rogers; 2006]

$$\rho_i = \frac{\sum_j \rho_j W_{ij} V_j}{\sum_j W_{ij} V_j} \quad (5.47)$$

Tensile correction

Tensile correction is required in the SPH method as it makes small clumps of particles due to negative pressure and the sign off the second derivative of the kernel function. The correction is activated with all kernels except the Quadratic and is build into the momentum equation (5.43) as it is demonstrated in equation (5.48). The scope of the correction is to induce a large repulsion between the particles when the particle distance decreases. The first spatial derivative of Quadratic kernel (5.6) is (unlike for instance the Cubic Spline kernel) always nonzero at the origin and it represents another approach to removing the instability. [Monaghan; 2000]

$$\frac{d\mathbf{v}_i}{dt} = \sum_{j=1}^N m_j \left(\frac{P_j}{\rho_j^2} + \frac{P_i}{\rho_i^2} + (R_i + R_j) f_{ij}^n \right) \nabla_i W_{ij} + \dots \quad (5.48)$$

$$f_{ij} = \frac{W(r_{ij})}{W(\Delta p)} \quad (5.49)$$

$$R_i = \frac{e|P_i|}{\rho_i^2} \quad (5.50)$$

where

$n > 0$ and equal to 2 in SPHysics F95 [-]

Δp is the average particle spacing in the area [m]

e is equal to 0.2 in SPHysics F95 [-]

r_{ij} is the distance between particle i and j [m]

5.2.6 Viscosity (Artificial & SPS Turbulence)

Traditionally, the viscosity terms in the SPH equation of momentum (5.52) have been described by an empirical term Π_{ij} (artificial viscosity) where α is an empirical coefficient between 0.01-0.1. The approach has several advantages as it represents viscosity, keeps particles from interpenetrating and keeps free surface flows numerically stable. However, critics say that it is too dissipative and affects the shear in the fluid. [Dalrymple and Rogers; 2006]

$$\frac{d\mathbf{u}_i}{dt} = -\sum_j m_j \left(\frac{P_i}{\rho_i^2} + \frac{P_j}{\rho_j^2} + \Pi_{ij} \right) \nabla_i W_{ij} + \mathbf{g} \quad (5.51)$$

$$\Pi_{ij} = \begin{cases} -\frac{\alpha \mu_{ij} \bar{c}_{ij}}{\rho_{ij}} & \mathbf{v}_{ij} \cdot \mathbf{r}_{ij} < 0 \\ 0 & \mathbf{v}_{ij} \cdot \mathbf{r}_{ij} > 0 \end{cases} \quad (5.52)$$

$$\mu_{ij} = \frac{h(\mathbf{u}_i - \mathbf{u}_j) \cdot (\mathbf{x}_i - \mathbf{x}_j)}{r_{ij}^2 + 0.01h^2} \quad (5.53)$$

The artificial viscosity approach is available in SPHysics together with an SPS (Sub Particle Scale) turbulence model where the viscosity is divided into two parts: The laminar viscosity and a SPS stress tensor τ^* representing the turbulent eddies smaller than the particle size. The SPH formulation is presented in equation (5.54) [Dalrymple et al; 2006] & [Gesteira et al; 2006]

$$\begin{aligned}
\frac{d\mathbf{u}_i}{dt} = & -\sum_j m_j \left(\frac{P_i}{\rho_i^2} + \frac{P_j}{\rho_j^2} \right) \nabla_i W_{ij} + \mathbf{g} \\
& + \sum_j m_j \left(\frac{4\mu_k \mathbf{r}_{ij} \mathbf{v}_{ij}}{(\rho_i + \rho_j) |\mathbf{r}_{ij}|^2} \right) \nabla_i W_{ij} \quad (\text{Laminar viscosity}) \\
& + \sum_j m_j \left(\frac{\tau_j^*}{\rho_j^2} + \frac{\tau_i^*}{\rho_i^2} \right) \nabla_i W_{ij} \quad (\text{SPS stress})
\end{aligned} \tag{5.54}$$

Both approaches have been used successfully to model 2-D waves breaking. The artificial viscosity approach is the more common approach as it is the oldest in use together with SPS first mentioned in [Monaghan; 1992]. A disadvantage with the SPH method is that it requires a Shepard filter (5.47) to be introduced as the inherent numerically stable surface is lost; but as it is only calculated once every 30 time steps it is of limited importance. No sources are presently found that make a detailed comparison of the two methods. This is not the scope of this project but it is decided to run a few simulations with each method for comparison.

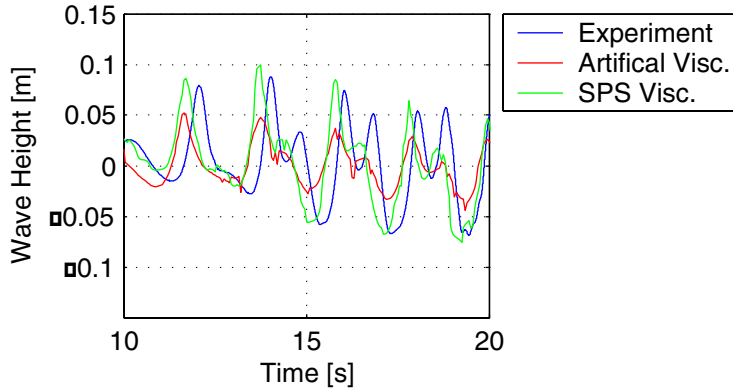


Figure 5.5. The depicted graph is a wave height comparison between values measured in the experiment of Appendix C and a corresponding virtual wave flume with two different approaches Artificial or SPS viscosity. The waves are measured 2 m from the end of a 16 m long flume.

To evaluate the quality of the two methods the sampled wave heights in the experiment of Appendix C are compared with two runs in the virtual flume, Section 5.3. There is no difference between the two virtual flumes except the use of Artificial viscosity (with $\alpha = 0.08$) or the SPS model. The comparison is depicted in Figure 5.5 and show that although the two methods initially agree about the wave height the waves modelled with artificial viscosity slowly dissipates. The solution of the artificial viscosity might be improved by lowering α and thereby decrease the artificial viscosity. But as the SPS run and the experimental values have a high level of correlation it is used for further modelling in this project.

5.2.7 Equation of state

When modelling fluids it is often safe to assume that the fluid is incompressible as the speed of sound in water c (≈ 1500 m/s) is many times higher than the speed of the bulk flow v for instance the speed of surface wave propagation. This is possible as the momentum equation leads to the relation in equation (5.55) where τ is the time scale and L is the length scale. The computed density variation is small i.e. the fluid is incompressible. [Monaghan; 1994]

$$\frac{\delta\rho}{\rho} = \frac{vL}{c^2\tau} \quad (5.55)$$

The reason not to treat the fluid as incompressible is to make it possible to use an Equation of state (5.56).

$$P_i = B \left[\left(\frac{\rho_i}{\rho_0} \right)^\gamma - 1 \right] \quad (5.56)$$

$$B = \frac{c_0^2 \rho_0}{\gamma} \quad (5.57)$$

$$c_0^2 = C_{coef}^2 g h_{SWL} \quad (5.58)$$

where

γ is a constant depending on the problem usually equal

to 7 when solving wave problems [-]

ρ_0 is the reference density equal to 1000 [kg/m³]

c_0 is the speed of sound at the reference density [m/s]

The Equation of state is included to describe the relation between the two state variables pressure and density. This is faster than solving an equation but also demands unreasonable small time steps in order solve the model, equation (5.67). The disadvantage is lessened by lowering the speed of sound, i.e. imposing an artificial/high compressibility. This works as long as the new speed of sound c_0 is much larger than the speed in the bulk flow. Sources like [Monaghan; 2004] recommend a minimum relation of $10v \approx c_0$ in order to keep density variation within 1 %. The parameter B is problem dependent and set a limit for the maximum change in density i.e. it decides the speed of sound. SPHysics estimates B using (5.57) and a estimate of c_0 , equation (5.58). In the estimate h_{SWL} is the mean water

level and C_{coef} is a coefficient which is recommend to have the limit $10 < C_{coef} < 40$. In most cases this provides $10v < c_0$. [Gesteira et al; 2007]

It has been decided to use C_{coef} equal to 16 i.e. a c_0 equal to 42.5 m/s and B equal to $25.8 \cdot 10^4$. This allows for a wave speed of 4.2 m/s and from Appendix C it is known that the wave speed in the flume based on period and wave length is max 2.5 m/s.

An incompressible SPH algorithm is not available with SPHysics but [Shao et al; 2006] worked with an incompressible approach where the pressure was calculated using a variant of the Poisson equation. It was showed by [Shao et al; 2006] that it was possible to simulate wave overtopping using this approach and although it meant larger computational effort at each time step it also allowed for larger steps as the speed of sound was no longer the deciding factor.

5.2.8 Time stepping (Verlet Algorithm and Δt)

Different time stepping schemes have been used with the SPH method. Traditionally the double step Predictor-Corrector scheme is the most common approach and it is, together with the single step Verlet scheme, the algorithms available in SPHysics F95. The Predictor-Corrector scheme represents another well known numerical scheme namely the Runge Kutta method that is used by [Colagrossi & Landrini; 2003].

It is decided to use the Verlet algorithm as a number of sources where similar SPH problems are investigated recommend it as stable and up to 50% faster than the Predictor Corrector algorithm. [Dalrymple & Rogers; 2006]

The Verlet scheme computes the variables every time step using the equations (5.59)-(5.62) where v_i is the speed and r_i is the position vector. [Gesteira et al; 2007]

$$v_i^{n+1} = v_i^{n-1} + 2\Delta t \left(\frac{dv_i}{dt} \right)^n \quad (5.59)$$

$$\rho_i^{n+1} = \rho_i^{n-1} + 2\Delta t \left(\frac{d\rho_i}{dt} \right)^n \quad (5.60)$$

$$r_i^{n+1} = r_i^n + \Delta t \left(\frac{dr_i}{dt} \right)^n + 0.5\Delta t^2 \left(\frac{dv_i}{dt} \right)^n \quad (5.61)$$

$$e_i^{n+1} = e_i^{n-1} + 2\Delta t \left(\frac{de_i}{dt} \right)^n \quad (5.62)$$

Once every M time steps (M equal to 30 in SPHysics) the variables are instead calculated using equation (5.63)-(5.66).

$$\mathbf{v}_i^{n+1} = \mathbf{v}_i^n + \Delta t \left(\frac{d\mathbf{v}_i}{dt} \right)^n \quad (5.63)$$

$$\rho_i^{n+1} = \rho_i^n + \Delta t \left(\frac{d\rho_i}{dt} \right)^n \quad (5.64)$$

$$\mathbf{r}_i^{n+1} = \mathbf{r}_i^n + \Delta t \left(\frac{d\mathbf{r}_i}{dt} \right)^n + 0.5\Delta t^2 \left(\frac{d^2\mathbf{r}_i}{dt^2} \right)^n \quad (5.65)$$

$$e_i^{n+1} = e_i^n + \Delta t \left(\frac{de_i}{dt} \right)^n \quad (5.66)$$

The size of the time step Δt is chosen during the geometry generation. The size of the time step must be proportional to the particle resolution i.e. the smoothing length and the maximum speed in the solution i.e. the speed of sound. With a constant value of h and a speed of sound from equation (5.58) this leads to (5.67). [Liu; 2003]

$$\Delta t = \min \left(\frac{h}{c} \right) \quad (5.67)$$

The maximum possible time step is estimated with two different tests. The Courant method (5.68) is a physical condition implemented to ensure that the solution is convergent. The Viscous method (5.69) is implemented to ensure a stable execution of the model [Shao et al; 2006]. The method is an integrated part of *SPHysicsgen F95* and keeping Δt beneath the recommended maximum allows a stable computation of the numerical solution.

$$\frac{c \Delta t}{\Delta x} < C \quad (5.68)$$

$$\Delta t = 0.125 \frac{h^2}{\nu} \quad (5.69)$$

where

C is the Courant number who recommend equal to 0.1 in SPHysics

The equations described above could also be used to allow Δt to vary during the numerical solution. This is possible as part of SPHysics F95 but it is experienced that using this possibility drastically increases the solution time.

5.2.9 Particle movement (XSPH correction)

Method used to move the particles. With XSPH a particle is moved with a velocity closer to the average velocity in its neighbourhood. It does not introduce dissipation but it increases the dispersion. It prevents particles with different velocities from occupying the same location and keeps fluids orderly in high speed flows (high Mach number). The variable e ($0 \leq e \leq 1$) is chosen as 0.5 in SPHysics F95 [Gesteira et al; 2007]. But the author of another SPH code [Liu; 2003] proposes a value of 0.3 (XSPH is turned off if $e=0$) for fluids with an open surface and values higher than 0.5 when modelling shock problems. The method is easily incorporated with equation (5.70). [Monaghan; 1989]

$$\frac{dx_i}{dt} = v_i - e \sum_j \frac{m_j}{\rho_j} v_{ij} W_{ij} \quad (5.70)$$

5.2.10 Particle interaction (Linked-list)

The linked list algorithm is used when searching for the nearest neighbouring particles to a particle i . The problem domain is meshed with a grid with a mesh spacing κh matching the dimension of the support domain i.e. the mesh depicted on Figure 5.6 would for instance work well with the Cubic Spline kernel because $\kappa = 2$. It is clear from Figure 5.6 that the particle only interacts with particles in its own and the eight neighbouring cells. It is not even necessary to search all eight neighbours as the interaction with four of the cells has already been resolved. This reduces the computational time from N^2 to $N \log N$ where N is the number of particles [Gesteira et al; 2007]. The linked list works best when the smoothing length is constant as it is in SPHysics. If a variable smoothing length was desired a better choice would be a Tree Search Algorithm. A solution tree is based on the particle position where the leaves of the tree are individual particles and the branches represent ever smaller volumes. The single particle/leave of course represents the smallest possible volume and by going back N branches the particle is in a support domain of arbitrary size $2\kappa h_i$. [Liu; 2003]

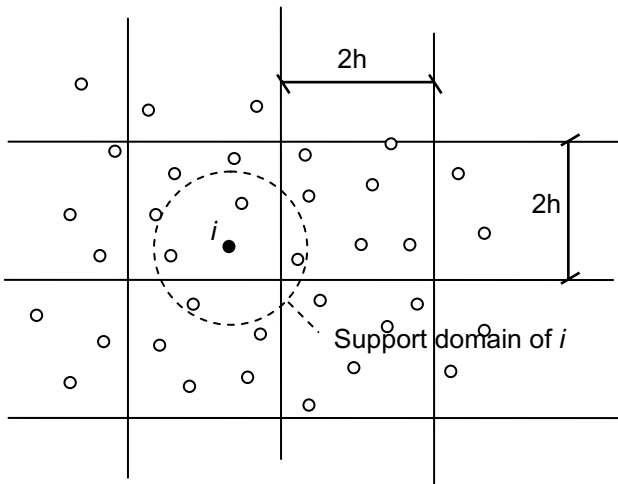


Figure 5.6. The principle of the Linked list search algorithm is depicted on this figure.

5.2.11 Boundaries

In Section 5.2.11 two different types of boundaries were described. Ghost particles placed on the other side of the boundary and repellent particles placed on the boundary. The boundary particles are both of the latter type although they use two different approaches to keep the particles within the boundaries.

- **Dynamics boundary conditions:** The boundary particles are part of the solution i.e. they are forced to satisfy the same equations as the fluid particles, Section 5.2.4 although they remain stationary. When a fluid particle approaches the wall the density increases due to equation (5.29) followed by an increase in pressure calculated with the equation of state (5.56). The result is a repulsion of the particles that begins when they reach within $2h$ of the wall. [Crespo et al; 2007]
- **Repulsive boundary condition:** The boundary particles are exerting a force \mathbf{f} normal to the boundary preventing any fluid particles from crossing the solid boundary. The method was refined by [Monaghan et al; 1999] and force is calculated using equation (5.71). The method needs to know the coordinates of the neighbouring boundary particles $i+1$ and $i-1$ to ensure a smooth travel parallel to the wall.

$$\mathbf{f} = nR_f(\psi)P(\xi)\varepsilon(z, u_\perp) \quad (5.71)$$

$$R_f(\psi) = \left(\frac{1}{h} 0.01c_i^2\right) \frac{1}{\sqrt{R}}(1-R) \quad (5.72)$$

$$R = \frac{\psi}{2h} \tag{5.73}$$

where

\mathbf{n} is the normal to the boundary at particle i [-]

ψ is the perpendicular distance between fluid particle and wall

$P(\xi)$ ensures that a particle travelling parallel to the wall experiences a constant repulsive force

$\varepsilon(z, u)$ adjusts the magnitude of the force according to water depth and fluid particle velocity

The principles of the two boundary conditions are depicted on Figure 5.7 together with an explanation of the two different ways to initially place particles in the model.

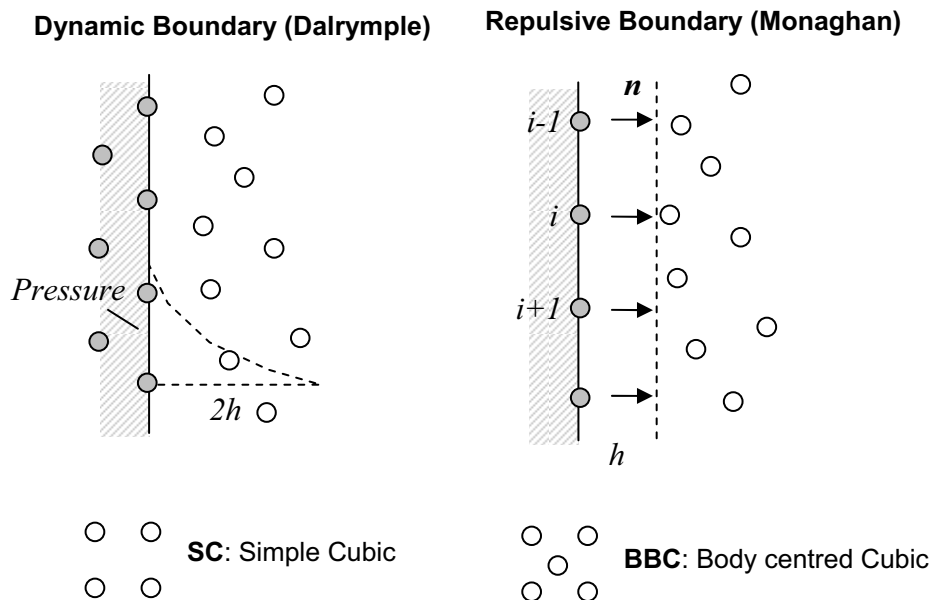


Figure 5.7. The two different boundary conditions available in SPHysics F95 the Dynamic boundary and the Repulsive boundary depicted together with two different initial particle distributions. BBC is mandatory together with the dynamic boundary.

Both boundary conditions have their cons and pros. The repulsive boundary particles approach is the oldest and the geometrically most versatile as it only demands a single line of particles making it easy to fit it to a needed geometry. One limit of the method is that the particles are not allowed closer than h to the wall as it is depicted on Figure 5.7 as the repulsive function at this point is fully activated $R(\psi) \approx$

1. This can be a problem with a large discretization. The method was used on a number of test cases and proved tight although particles might escape at the corners if two boundaries overlap or are too far apart.

The dynamic boundary uses the inherent property of the SPH method that two particles repulse each other and if one is kept fixed in space the other will not pass it. This is the strength of the method as unlike the repulsive approach all calculation is kept within the same loop as the fluid particles it is not necessary to calculate a repulsive function and the normal. The fact that the particles are part of the boundary and the fluid particle solution means that it is easy to measure pressure at different points on the boundary. The problem of the method is the two layers of boundary particles which make it harder to build geometry with many intersections.

It was chosen to build the fluid geometry using the repulsive boundary approach mainly because it was the easiest way to model the geometry but also because problems were experienced with dynamic boundaries at the time of the decision depicted on Figure 5.8. On Figure 5.8 the particles are escaping through the tilted wall and will eventually drain the box. This escape through a tilted plane would make the boundary useless in a virtual wave flume and due to the time available it was decided to concentrate effort on repulsive boundaries as it with the right discretization would be possible to get a good picture of the pressure at the boundary although it would not be possible to measure pressure at the boundary particles themselves.

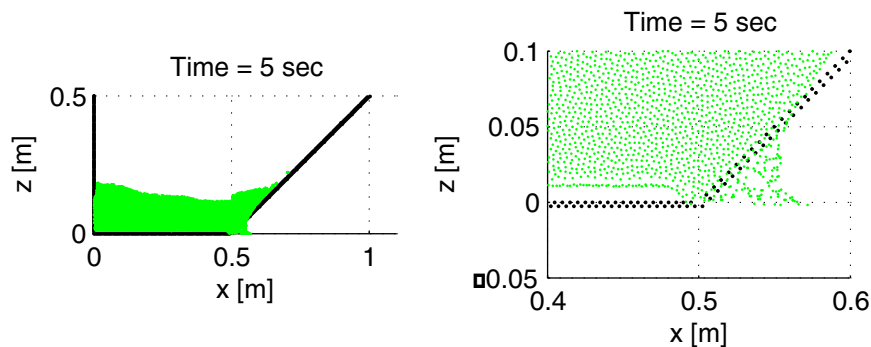


Figure 5.8. Problems with the Dalrymple boundary conditions. Particles are leaving the problem domain. To the left the whole problem area is depicted and to the right is a close up of the problem. The simulation is available on the CD

A particle escaping through the boundary is possible with both boundary methods and is only a question about the particle speed $|\mathbf{v}_i|$ being large enough. When choosing boundaries it had only been experienced with dynamic boundaries but in

later simulations the problem appeared with repulsive boundaries. This is further discussed in Section 5.4.

According to [Gesteira et al; 2007] the present version of SPHysics F77 should also be able to handle periodic open boundaries but this is only possible with the 3-D source code. It might become available in a later edition but if that is not the case another source would be [Rogers; 2008] who made a webpage on the subject: Open boundaries and SPH.

5.3 Virtual wave flume – The model

The virtual wave flume is build using SPHysics F95 described in Appendix B together with the customized version of SPHysicsgen F95 used to initiate the model. The virtual flume is build to match the geometry of a flume at Aalborg University henceforward referred to as the real wave flume the geometry of this flume is described in Appendix B.4 and depicted in Figure 5.10.

Table 5.3. The key SPH parameters chosen when building the virtual flume. The input files to generate geometry and initial conditions are available on the CD-Rom.

Geometry	Fluid	Time stepping
Particle spacing (SC) [m] 0.02	SPS viscosity μ_k [m ² /s] 10^{-6}	Time stepping [s] $4E10^{-5}$
Smoothing length k_h [m] 0.92	Shephard filter - -	Output step [s] 0.05
Dynamic boundary - -	B [kg/ms ²] $25.9E4$	Run time [s] 30
	γ [-] 7	Verlet algorithm - -

When building the flume a number of choices were made on how to use the different SPH parameters. The chosen variables used in the virtual flume are listed in Table 5.3 and the following choices were made with regard to different SPH methods: To speed things up the Verlet algorithm is used for the numerical time integration. The wave flume geometry is build using dynamic boundaries and the SC distribution of particles. The turbulence is modelled using both approaches described in Section 5.2.6 together with a Shephard filtering to ensure a smoothed surface. In the experiments a structure consisting of a wall and a platform is present at the end of the wave flume this is also modelled with the boundary particles. The particle approximation is done using the Cubic Spline kernel. To generate the paddle movement a sampled time series from the experiments in the real flume is loaded. The experiments and the comparison between the samples in the virtual and the real flume are further discussed in 0.

5.3. Virtual wave flume – The model

The initial distribution of particles and their particle variables velocity v_i (x and z), density ρ_i , pressure P_i and mass m_i are all computed in SPHysicsgen F95. The initial velocity is zero and the particle mass is a constant for all particles while the density and pressure are distributed like depicted in Figure 5.9 for a part of the flume. The density for water ρ_0 is equal to 1000 kg/m^3 but as SPHysics is working with a compressible fluid the density is calculated using B and the initial pressure is found with the Equation of State.

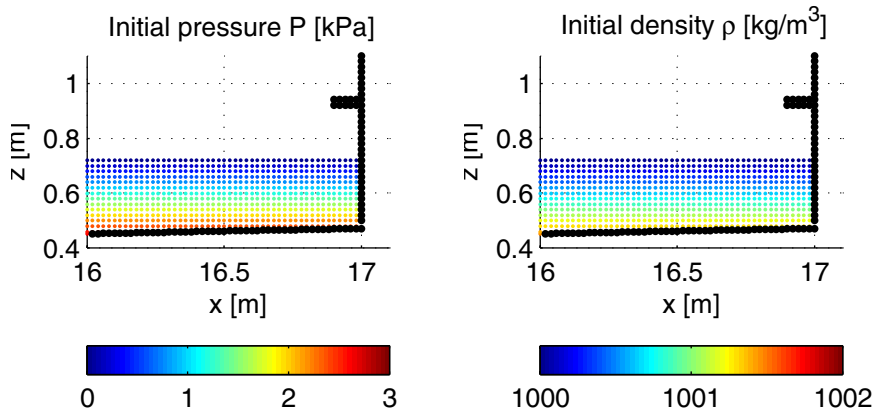


Figure 5.9. The initial distribution of hydrostatic pressure and density at the end of the virtual flume generated by SPHysicsgen F95. The distribution is the same in the remaining part of the flume.

The virtual wave flume is finally depicted in Figure 5.10 having modelled 15 seconds of waves using the SPH parameters listed in Table 5.3.

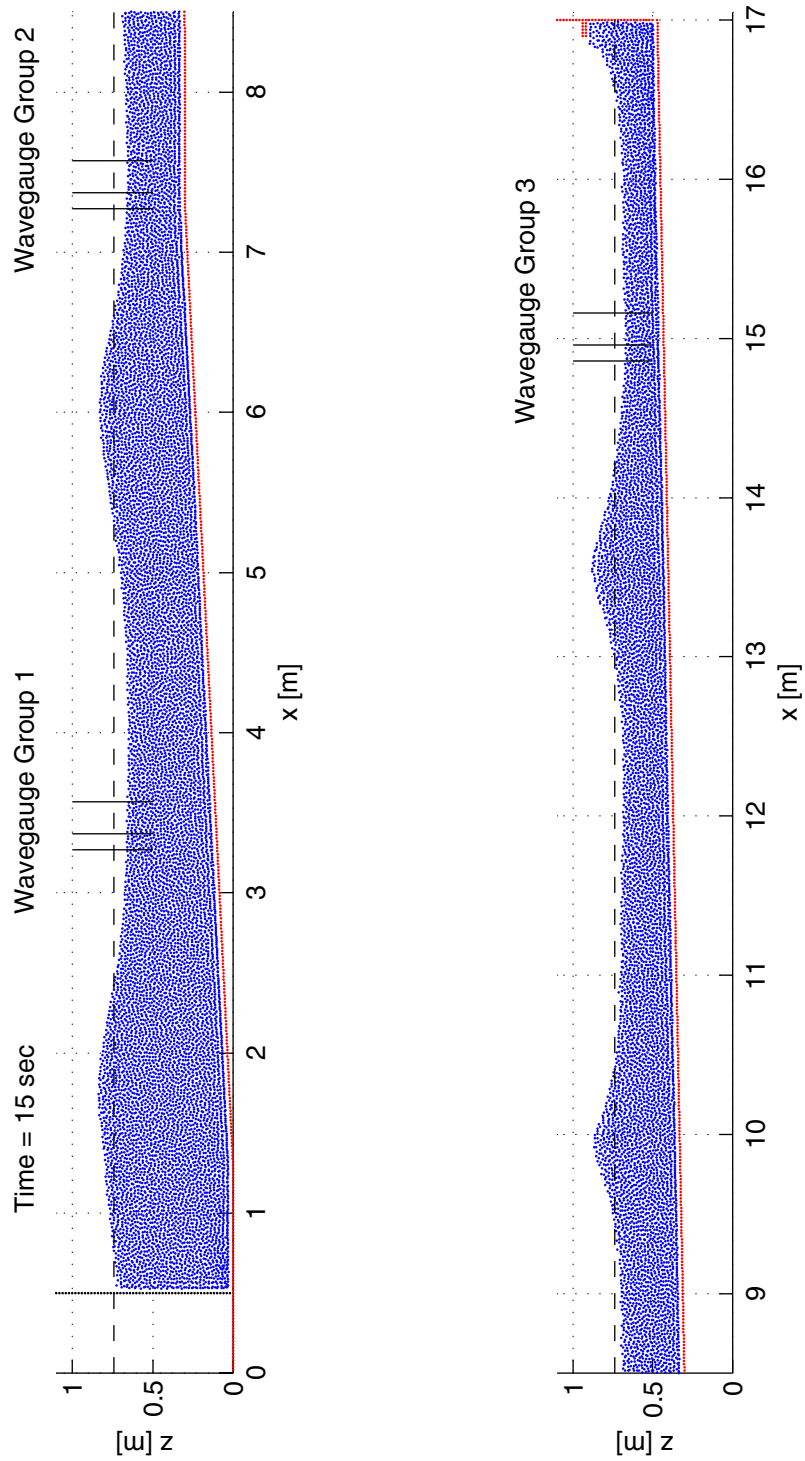


Figure 5.10. The geometry of the virtual wave flume used in this project depicted after 15 seconds of wave generation using a sampled paddle movement. The initial SWL is depicted as a dotted line together with the location of the wave gauges used to measure wave height in the real flume.

5.4 Test of SPHysics F95

The SPHysics F95 code rewritten from the original SPHysics basis is tested. Before conducting this it has been verified that SPHysics F95 is able to solve the 2-D test cases presented by [Gesteira et al; 2007].

5.4.1 Collapsing column

The classic SPH example: The collapsing column, cf. Figure 5.12. The idea is to let the water from a collapsing column fill a box with an inclined bottom in order to test if the method computes the correct pressure distribution and how it evaluates kinetic and potential energy. The problem in the basis form is evaluated with SPS turbulence, Quadratic kernel functions and a discretization where $dx = dz = 0.005$ m.

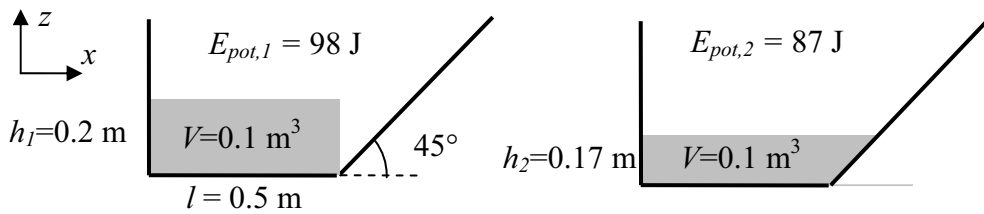


Figure 5.11. To the left the water column before the collapse is depicted and to the right is the same volume of water after the collapse. The potential energy before and after is easily calculated using the depicted dimensions.

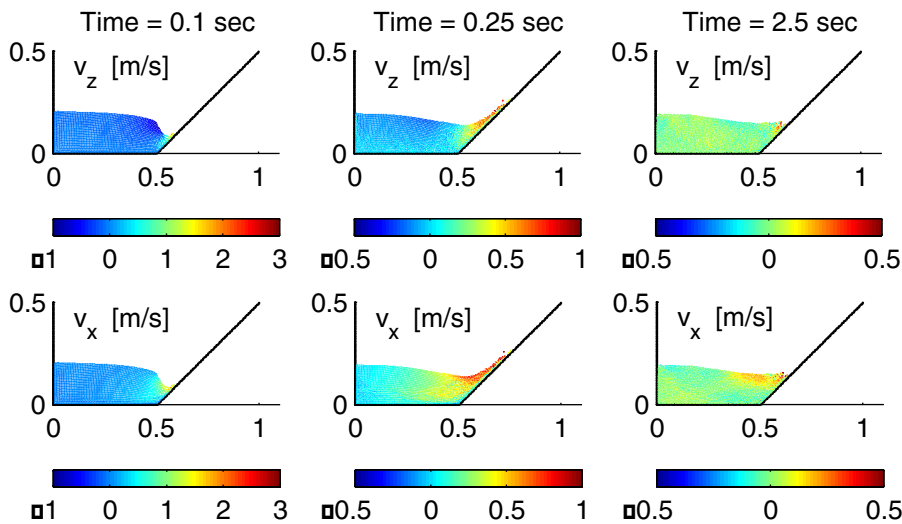


Figure 5.12. The Collapsing column example is used to test SPHysics F95 in three different time steps showing how when the column of water collapses a new equilibrium is established.

The potential E_{pot} and kinematic E_{kin} energy is easily computed using the known particle position and velocity in each time step. The result is depicted as a graph in Figure 5.13 together with the thermal energy E_{term} computed during the solution in SPHysics using the energy expression of Box 5.1.

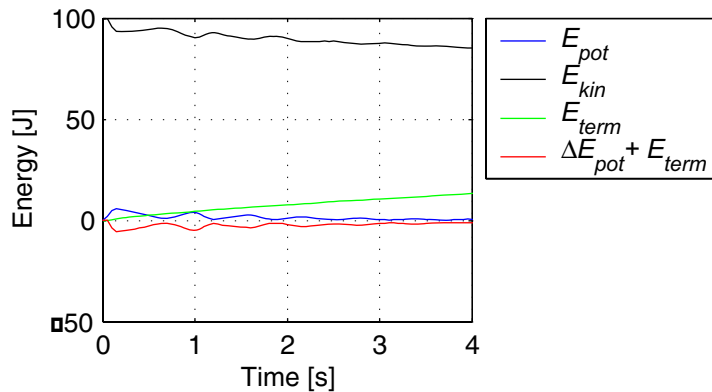


Figure 5.13. The total potential, kinematic and heat energy in the collapsing column in the first four seconds of the solution depicted as a graph where ΔE_{pot} is the change in potential energy in relation to the original level.

It is evident from the depicted graph that there is a good agreement in the evaluation of the three forms of energy in the first four seconds. However this is only the first four seconds of the plot and problems was experienced with the SPHysics code if problems ran more than a few seconds. These problems are discussed in the next Section.

5.4.2 SPHysics – Crash of computation

The test case used to validate that the changes in SPHysics are working show that the program is able to evaluate fluid problems and maintain a balance between the three types of energy in the system. The problem is that the models crash after a problem dependent number of time steps. The particle distribution just before the crash is depicted on Figure 5.14.

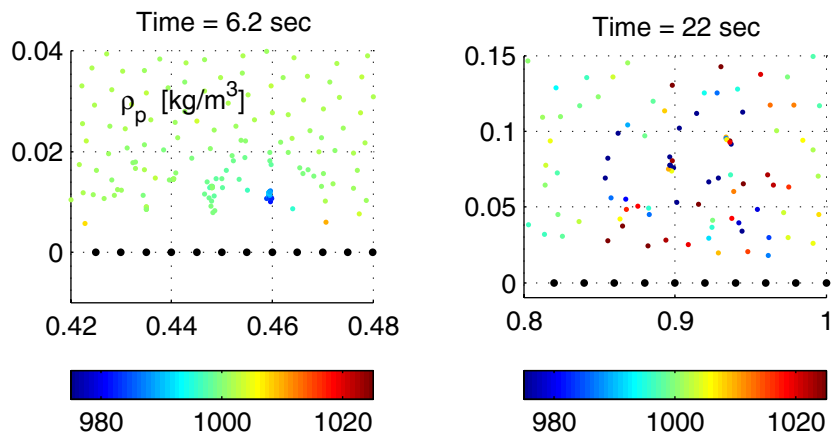


Figure 5.14. To the left is a close up on the collapsing column and to the right is a close up on a part of the virtual flume with the standard parameters given in Section 5.3. Both particle plots are from a few time steps before a crash in the computation and in both situations the density is distorted in a small area of the solution.

Particles in a small area clod and this changes the approximated density and velocity of a few particles allowing them to pass through the boundary and escape the problem domain. After the escape of the first few the remaining follows. When the problem occurs it depend on the initial particle spacing and what kind of problem is computed. The virtual wave flume is able to compute app. 28 seconds of wave movement while the collapsing column experiences problems earlier during the run. Based of this it is speculated that the problem initiates from a change in particle position/density that the Continuity equation and the Equation of state are not able to compute.

The problems appear similar to the tensile instability described in the SPH literature where the particles form clods but this should have been removed either by using the Quadratic kernel or using tensile correction as discussed on page 61 [Monaghan; 2000]. Both methods have been used in the collapsing column but it only changes when the clod appears.

When the problem was identified a number of different approaches were done within the limit of the code in order to detect whether the crash was due to an error in the code or due to a limit in the used SPH tools. The following items did not change anything.

- The same code has been run in SPHysics F77 with the same results.

- Tried to change the way turbulence was evaluated from SPS to artificial viscosity with α equal to
- Different kernels were used. It changed when the crash occurred but not how.
- The variable γ in the equation of state was changed to 3.5 it limited the problem to a smaller area but still allowed the particles to accumulate density.
- The problem was evaluated with Double precision variables instead of Single precision.
- The time integration was changed from the Verlet Algorithm to the Predictor corrector scheme.

The only thing that did work was a change in the discretization. With a particle spacing of 0.025 m (and the same choices in time stepping) it was possible to allow the problem to be computed in 15+ seconds. This indicates that there is not anything fundamentally wrong with the source code of SPHysics F95 and the problem is more likely due to an error in the numerical integration. A way to solve the problem would be to use even smaller time steps but as it already takes a week to model the virtual flume this is not an option.

5.5 Sub Conclusion

In this chapter the virtual wave flume has been constructed and the theory it based upon has been derived. The combination of methods is chosen based on the experience gained during the project and the comparison between virtual and real flume in the next chapter will show if they are right. To further improve understanding of SPH it would be beneficial to compare it with other CFD solvers and compare results.

The virtual wave flume described in Section 5.3 is able to run in minimum 22 seconds before the tensile instability causes the code to crash. This is enough time to compare with experiments although it is not possible to use discretization lower than 0.02 m as the computation time would be too long (SC distribution). The flume contains app. 20,000 particles and takes 5 days to compute with the best available computer. There has not been time enough to determine for certain why the SPH code becomes unstable but the problems does not affect the overall results from the flume as they are limited to a small area of particles.

Chapter 6

Virtual versus Real Wave flume

Using the virtual wave flume presented in the previous chapter the numerical results are compared with measurements on the real wave flume in the Wave Laboratory at Aalborg University. The two flumes are compared on two different levels

- Waves: The generated waves are measured at three different locations in the flume in order to compare the real and virtual wave picture.
- Wave impact: At the end of the wave flume the wave impact on a structure is measured using pressure transducers.



Figure 6.1. To the left is the inspiration for the experiments depicted: A platform on the substructure of a wind turbine. To the right the simplified structure is used in the experiments depicted.

The inspiration for the experiment was the wave impact situation when waves hit an offshore wind turbine and the platform on the substructure depicted on Figure 6.1. A simple 2-D experimental setup was devised to investigate if the method could be used to model this kind of impact problem.

6.1 The Experiment

The purpose of the experiments was to get a source of reference when using the program SPHysics F95 to compute a virtual wave flume. Therefore it was the intention of the experiments to generate a similar situation in a wave flume with waves breaking against a vertical structure and hitting a platform. The work of building a virtual SPH model of the flume and comparing with the experiment will expose the current limits of the SPH method and clarify how well the method is able to model two-dimensional (2-D) wave flume with distortion of the free surface, impact against structures and turbulence. The experimental setup and processing of the results is presented in Appendix C.

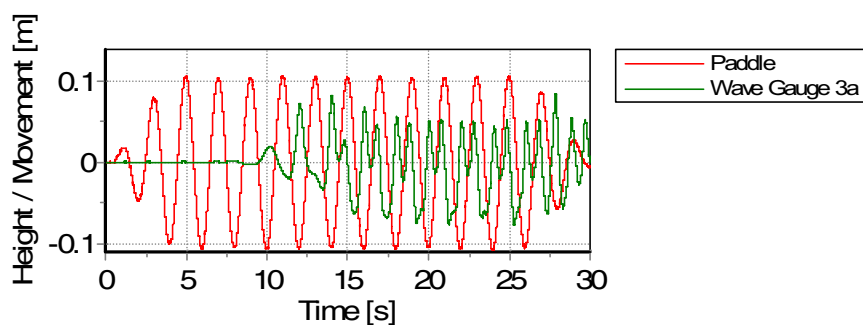


Figure 6.2. A measured time series of the paddle movement generating the waves and the waves measured just before the structure. The plotted wave initially have $H_m = 0.12$ m and $T_m = 2$ sec.

In a typical experiment the waves were generated by the paddle at one end of the flume and travelled down the flume until they were reflected by the structure depicted on Figure 6.1. A time series of the paddle movement and the generated waves measured just before the structure is depicted on Figure 6.2. The nine wave gauges used to measure the wave height in the flume are placed in three groups (1, 2 & 3) the exact position is depicted on the virtual flume in Figure 5.10 and in Appendix C.4.2.

On Figure 6.3 the transducers are used to measure the impact depicted together with a list of transducer numbers used in the experiment. Two different types of transducers with different sizes were used ($\varnothing 8$ and $\varnothing 19$). Before beginning the experiments a number of samples were taken in order to determine the reliability of the measurements. It showed that for everything but the peak values there was a high level of correlation (more than 92 %) between two measured time series on the same transducer, Appendix C.6.1. The measured mean peak value is depicted together with its standard deviation in Figure 6.4 it shows that the transducers at the intersection between the wall and the platform have the highest level of deviation.

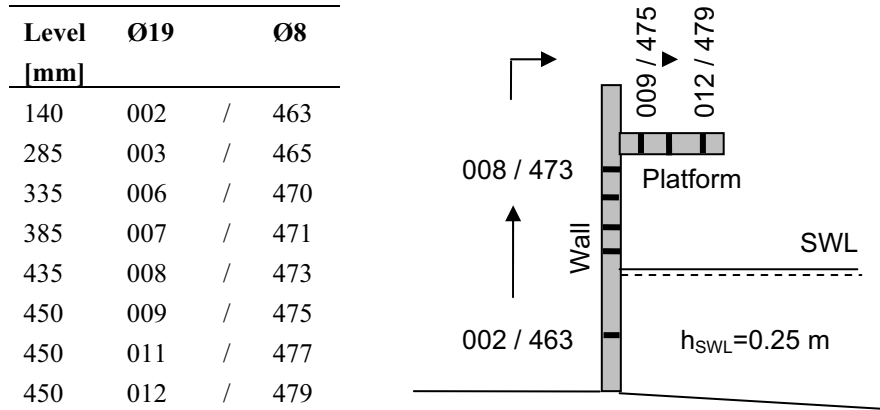


Figure 6.3. To the left a list of the pressure transducers used to measure the impact and to the right an outline of the structure build at the end of the flume.

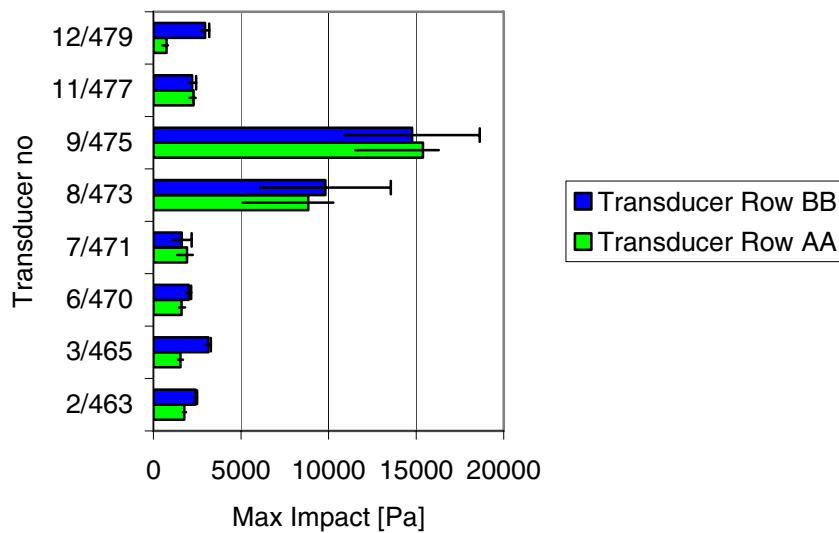


Figure 6.4. The maximum impact measured when testing the reliability of the setup and the corresponding standard deviation s_{Max} computed in Appendix C.6.1.

The post processing of the experimental measurements show that the impact on a structure of the type used in this experiment happens instantaneous and with the highest level of impact at Transducer no. 8 and 9. A number of different regular wave series was generated during the experiments but only a few will be subject to further comparison in this chapter, cf. Table 6.1. It was discovered that the size of the impact and the wave height was closely connected and that the combination of air, water and the structure enhances the impact and introduces a degree of un-

6.2. Comparison of generated Waves

predictability. As the air is not present in the virtual flume it is expected that there will be a difference between the peak values measured in the real and virtual flume.

Table 6.1. The wave height and period measured at the first group of wave gauges used to compare the virtual and the real flume. The name refers to the description in Appendix C.

Name	Wave height H_m	Wave period T_m
	[m]	[s]
Exp 2 – Run no. 5	0.15	2

6.2 Comparison of generated Waves

It is possible to compare the wave height H and period T at three different positions in the wave flume depicted on Figure 5.10. The basis flume parameters listed in Table 5.3 are used to model the virtual flume with waves generated by the sampled paddle movement.

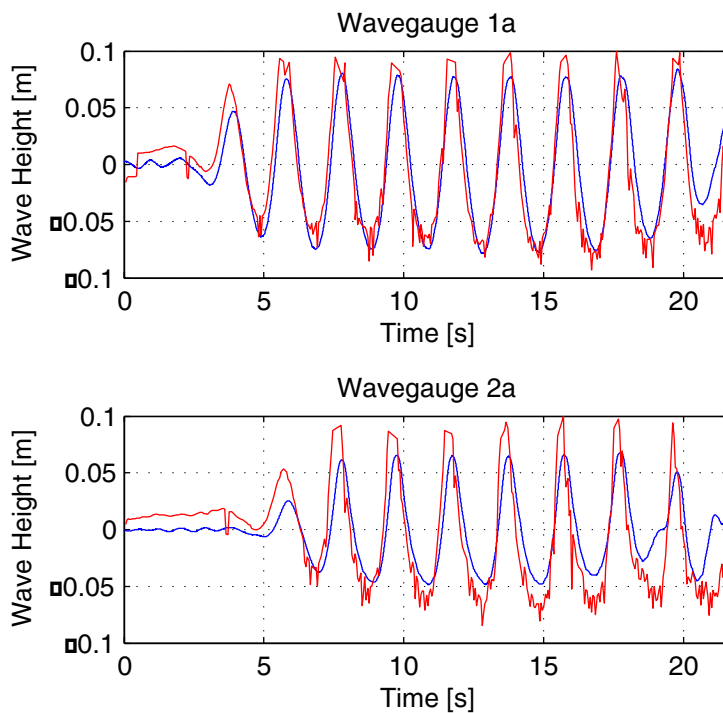


Figure 6.5. Comparison of the wave waves measured at the two first wave gauge locations. The real and virtual flume is based on Run no. 5.

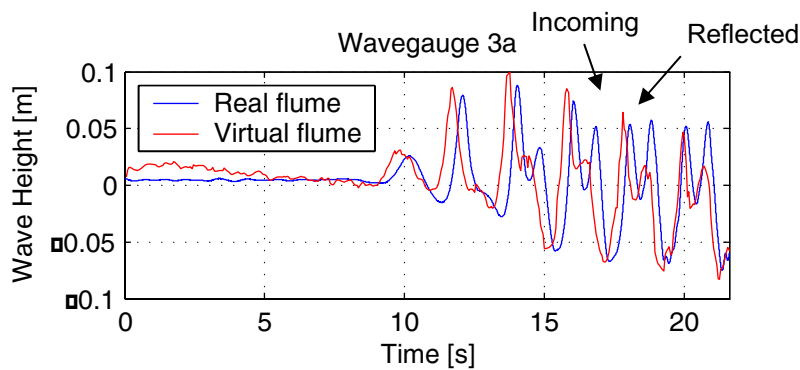


Figure 6.6. Comparison of the measured wave waves at the third of the three wave gauge locations. The real and virtual flume is based on Run no. 5.

The second comparison is based on Run no. 5 where a series of regular waves are generated with H_m equal to 0.15 m and T equal to 2.0. The depicted measurements in Figure 6.6 show that there is a good agreement between the virtual and real waves. Some of the differences between them are explained by the way water elevation is measured in the virtual flume where the particle with the highest z -coordinate is selected to represent the surface and particle spacing of 0.02 m will lead to error when measuring a wave height of 0.1 m. It is evident that the two flumes agree about the period and height of the incoming waves. It is in the wave reflection measured at Wave gauge no. 3a that differences start to emerge. The incoming waves are represented by the first crest and the reflected waves are the second crest. Figure 6.6 shows that the reflection is smaller in the virtual flume.

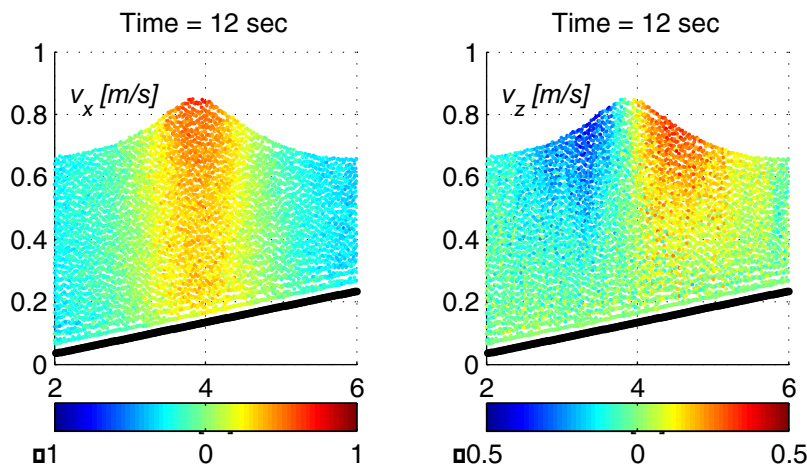


Figure 6.7. The wave velocity field at Wave group no. 1. The waves are generated to resemble the waves in Run no. 4.

6.2. Comparison of generated Waves

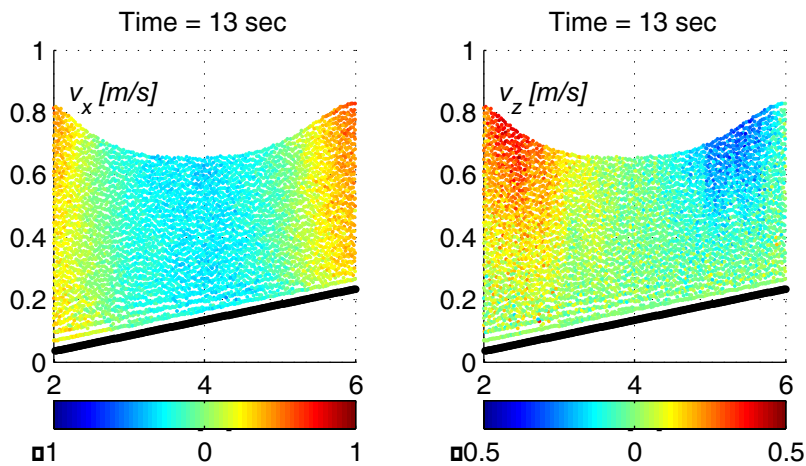


Figure 6.8. The wave velocity field at Wave group no. 1. The waves are generated to resemble the waves in Run no. 4.

The velocity field depicted on Figure 6.8 shows that the virtual flume models the expected velocity pattern with maximum v_z on each side of the crest and maximum v_x on top of the crest. By using the real measurement at Wave gauge no. 1a to calculate the expected wave speed it is possible to calculate the expected particle speed in 5th Stokes waves with WaveLab ($H/L < 0.01$), cf. Table 6.2.

Table 6.2 The wave velocity at Wave gauge no. 1a based on 5th order Stokes waves and the measured wave height and period in Run no. 5. The virtual wave flume speed is taken from the area depicted on Figure 6.8.

Real flume			5 th order Stokes				Virtual flume	
H_m	T_m	h_{SWL}	L_m	c	$v_{x,max}$	$v_{z,max}$	$v_{x,max}$	$v_{z,max}$
[m]	[s]	[m]	[m]	[m/s]	[m/s]	[m/s]	[m/s]	[m/s]
0.15	2	0.5	4.2	2.35	0.49	0.26	0.65	-0.45

The comparison shows that if the wave height and water depth at the wave gauges are used there is difference between the 5th order waves and the virtual flume. But as it is depicted on Figure 6.9 shoaling raises the wave crest and shortens the wave length. The used 5th order waves are based on a horizontal bottom and by changing the premise of the calculation slightly it is possible to get even closer to the result in the virtual flume. It would be best to compare a virtual flume with a plane bottom with the 5th order waves but there was not time for this before the project closure.

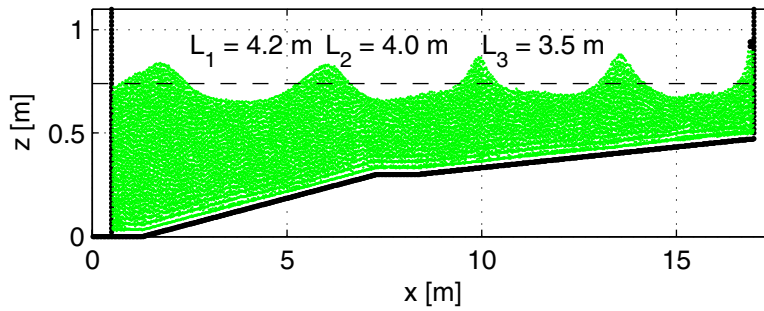


Figure 6.9. Waves in the virtual wave flume after 15 seconds with $H_m = 0.12$ m and $T_m = 2$ seconds. The wave length of the three waves is measured between the crests.

6.3 Comparison of wave impact

The impact between structure and wall is compared at the pressure transducers placed as depicted in Figure 6.3. Due to the choice in boundary conditions it is not possible to measure the pressure directly on the boundary but rather on the particles right next to it. A typical boundary history is depicted on Figure 6.10 where pictures taken in the laboratory is compared to measurements from the virtual flume.

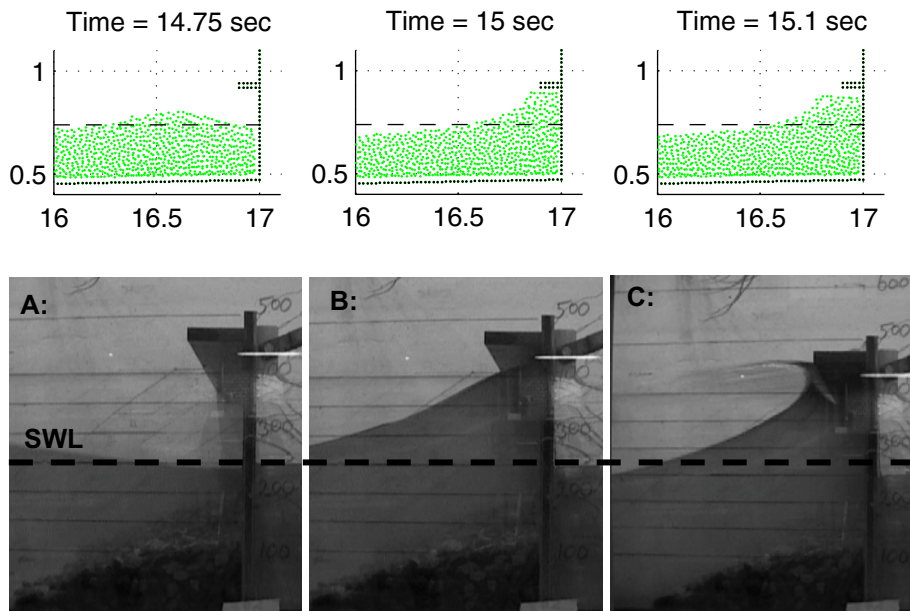


Figure 6.10. The impact of the structure depicted in a series of pictures from just before to just after impact. The particle position in the virtual flume and pictures from the real flume are paired together. The dotted line shows the original SWL.

6.3. Comparison of wave impact

It is evident from the visual comparison of the impact in the real and virtual flume, that there is good agreement between how the water is distributed during the impact. It was not possible to generate the same long violent splash of water backwards from the structure evident on Figure 6.10C but this is properly due to the size of the individual particles. The next step is to present the experimental results of a single impact chosen from Run no. 4 and 5. The waves and structure impact several times during the experiment and only one chosen for comparison as the general impact history is the same and there is a high level of correlation between the measurements. The impact is depicted in Figure 6.11 and the transducer location is depicted in Figure 6.3 or Appendix C.4

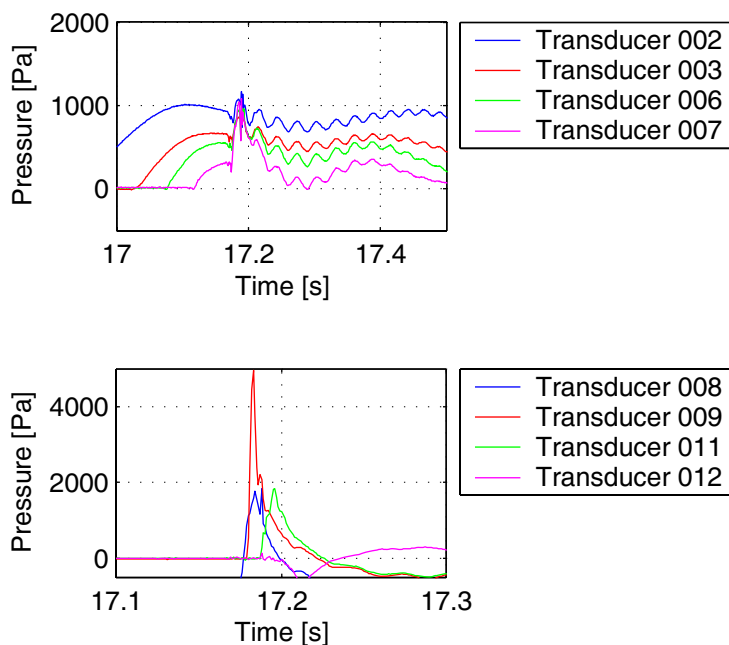


Figure 6.11. Impact history of a single impact in Run 5 measured with the transducer Ø18. The impact is part of a series of impacts generated by the regular waves. Note the difference in the timescale between the upper and lower plot.

There is an evident difference in the impact size between the transducers. The transducers placed at the intersection between platform and wall measure by far the greatest difference in pressure. The plot is now compared with the virtual flume at four different time steps, cf. Figure 6.12. From Figure 6.6 it is evident that there is a slight delay between the virtual and real measurements app. 0.5 seconds.

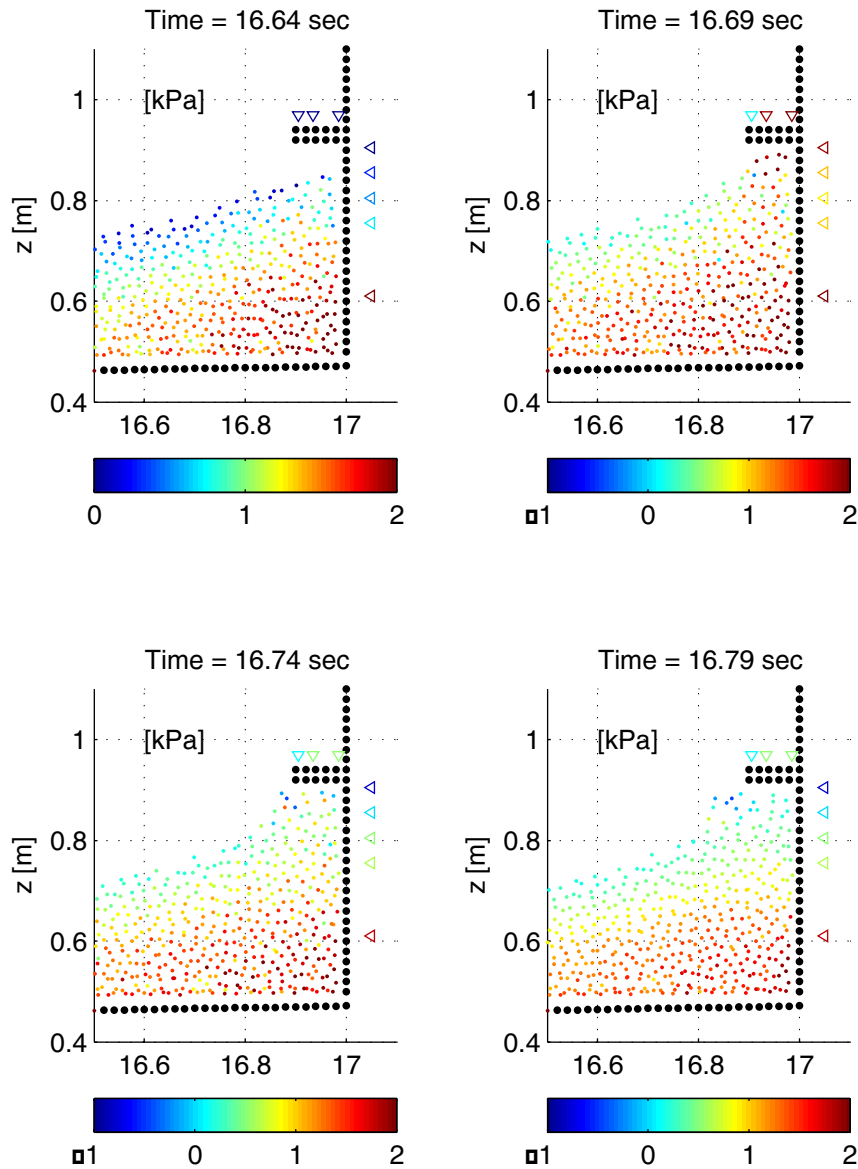


Figure 6.12. The pressure at the structure computed in the virtual flume and compared with the experimental results depicted in Figure 6.11 with an initial wave height of Run no 5. The transducer location is marked by a wedge (\blacktriangleleft or \blacktriangleright). Notice the difference in pressure scale.

The impact history of Figure 6.12 show that it is hard to compare the impact pressure with the current virtual flume as the discretization is low. It seems nevertheless that the virtual flume is able to model a rough picture comparable to the real.

6.4 Sub conclusion

The comparison of the virtual and the real wave flume shows that there is a high level of agreement between the size and shape of the generated waves. The virtual solution would properly benefit from a higher level of discretization especially around the end of the flume where the pressure at impact is hard to determine. It is certain that with the current discretization the measured virtual impact is smaller than the real one although one could speculate that more energy is being lost in the virtual impact due to the diminished size of the reflected waves, cf. Figure 6.6.

It has earlier been speculated whether the Dalrymple boundary conditions would work better than the used dynamics approach when modelling this kind of problems. This is probably true as it would be possible to measure directly at the boundary but a higher level of discretization would still be needed.

Only a small number of the experimental runs were chosen for comparison with the virtual wave flume and the field was further diminished by the available time and the problems to create a virtual flume running long enough to be able to compare the results. With the chosen comparison between experiment and numerical model it has been made probable that the virtual flume is able to generate results similar to the real thing measured in the wave laboratory at AAU.

Chapter 7

Conclusion

The SPH method has since its introduction to CFD problems in 1992 been through a major development in order to optimize its ability to compute fluids. There are now a number of different ways to combine the supplement methods added the last 15 years and in this report one approach in the form of SPHysics 1.0 has been used. The basis of these different approaches remains the same and it is this basis that is described in the first part of the report. No matter how the different filters and algorithms are combined will the choice in kernel function and smoothing length be the tools that ultimately solve the field functions. The test cases of the first few chapters show how small alterations to the smoothing length or a different choice in kernel can change the solution. The supplement methods have been added later to improve the solution and ensure the right physical solution of the fluid. They are described in the second part of the report together with the virtual flume and represent the basic approach normally used with SPH. It has been shown that this combination works although it does not guarantee a working solution shown by the problems in the computation.

The program SPHysics used to build the virtual flume is only one possible way to combine the different SPH methods. SPHysics became available in July 2007 just when it was needed in the project and it was chosen to use SPHysics rather than build a new program from scratch because of its wide range of possibilities. Subsequently a lot of time has been used to understand how an advanced SPH program like SPHysics is working and although there is still room for improvement the source code has been organized using the newest possibilities available with Fortran and rebuilt to model the virtual copy of a wave flume at Aalborg University.

Only a small part of the experiment described in the Appendix has been compared to computational results in this report. But as it was shown in the post processing of the experiments are the time series consisting of a series of similar impacts with

7.1. Further work on the Virtual Wave Flume

a regular wave pattern in the flume. The measurements have a high level of correlation except at the peak values therefore a lengthy comparison with all the different combinations of wave conditions would not present any surprises. It would have been of interest to generate waves breaking before reaching the structure in the virtual flume in order to validate the SPH ability to generate the crest of the waves at the point of overtopping. It has been shown by comparison between the real and virtual flume that the computed wave pattern match the one measured in the experiments and that the particle speed in the wave match the pattern presented by the wave theory. The impact of the structure was difficult to measure given the boundary choices when building the virtual flume and the limits of the program itself. It is evident that the particles are modelling the kinematics of the impact correctly and reflects the waves but due to the relatively rough discretization in this part of the flume it was not possible to validate if the pressure at the structure was corresponding to the experimental values.

If more time was available would it be interesting to take the experimental data at hand and begin a parameters study of the major input variables in SPHysics controlling the speed of sound, turbulence and particle distribution. With ample time and computational power available it would also be possible to increase the discretization of the virtual flume and get better readings on the generated wave impact. A prerequisite of this would of course be to determine why exactly the computation has a tendency to crash.

The conclusion of this project is the SPH method is in fact a good choice when modelling a virtual wave flume and that the method is able to handle CFD problems with breaking waves and impact against a structure. But one needs to combine the right SPH tools to get the optimum solution and in that respect a number of possibilities remain for future projects.

7.1 Further work on the Virtual Wave Flume

There is much yet to be done with the SPH method as it has not been subject to the same amount of research as more traditional methods like FEM and FD. This Section will list some of the items it would be interesting to implement in the code if more time was available.

First of all it needs to be determined if the instability problems with SPHysics F95 was due to some error in the source code or an example of tensile instability. If the problem is due to tensile instability it is evident that the methods used in this project as countermeasures need to be further enhanced. It would furthermore be beneficial to clean up the code and rebuild the geometry generation.

A rewriting of the 3-D version of SPHysics along the same lines as the 2-D version would be a logical next step in order to compute models of a wave basin with a 3-D wave pattern. With the SPHysics 3-D in place it would also be possible to conduct a real study of the wave impact beneath the platform of an offshore wind turbine.

The rewritten 3-D version of the code would also demand an increase in the computational processing power as a computation with 20,000+ particles presently takes more than a week. It was early discovered that the SPH method does not demand a lot of memory in the present explicit form instead it needs a lot of processing power because of the small time steps. The implementation of parallel processing on more than one processor might make this possible.

SPHysics does not currently work with a compressible approach to the Navier-Stokes solutions but it is possible to generate SPH formulation based on an incompressible approach. This requires an implicit solution of the pressure each time step but it also allows for larger time steps and it might be interesting to investigate if this formulation is more stable.

The above mentioned is only a few of the things that could be done to further improve SPHysics and it must furthermore be expected that the original authors of SPHysics 1.0 will release another edition in a few years.

7.2 Other possible SPH problems

During the project other possible uses of the SPH code has been discussed apart from the impact problem used in this project. One possibility would be to use the method to compute overtopping not just across a regular breakwater but also in wave power constructions like the wave dragon where energy is created by overtopping into the basin on top of the structure, cf. Figure 7.1. With SPH it would be possible to measure the amount of water (particles) entering the basin with a given wave climate.

A possibility with particle methods not previously mentioned in this report is to have an object “float” in the particles. This would for instance be of interest with the wave star project where methods are needed to optimize the size and shape of the floaters on which the structure rest, cf. Figure 7.1. According to the researchers presently working on the project this is not possible to model with the available numerical and analytical methods.

7.2. Other possible SPH problems



Figure 7.1. Future examples of how the SPH method or other particle methods could be utilized. To the left is the Wave star [Wave star; 2008] and to the right the Wave dragon [Wave dragon; 2008].

Chapter 8

List of references

Technical literature

- [Brorsen; 2005] Brorsen, M., 2005. *Strømningslære*, Institute for Water, earth and environmental science, Aalborg University
- [Chapman; 2004] Chapman, S. J., 2004. *Fortran 95/2003 for scientists and engineers*, 3rd edition, McGraw-Hill, New York, ISBN: 978-0-07-319157-7
- [Liu; 2003] Liu, G. R., 2003. *Smoothed Particle Hydrodynamics: A Meshfree Particle Method*, World Scientific Publishing Company, Singapore, ISBN: 981-2384561
- [Nielsen; 2007] Nielsen, S. R. K., 2007. *Vibration theory, vol. 3: Linear Stochastic Vibration Theory*, 3rd edition, Aalborg Tekniske Universitetsforlag, ISSN: 1395-8232 U0007
- [Vesely; 2001] Vesely, F.J., 2001. *Computational physics – An introduction*, Klüwer Academic/Plenum Publishers, ISBN 0-306-46631-7
- [Zill & Cullen; 2001] Zill, D.G., Cullen, M.R., 2001. *Differential equations with boundary-value problems*, 5th edition, Brooks/Cole, ISBN: 0-543-38002-6

Scientific articles

- [Antoci et. al; 2007] Antoci, C., Gallati, M., Sibilla, S., 2007. ‘Numerical simulation of fluid structure interaction by SPH’, *Computers and Structures*, vol. 85, pp. 879-890

7.2. Other possible SPH problems

- [Bonet & Kulasegaram; 2000] Bonet, J., Kulasegaram, S., 2000. 'Correction and stabilization of smooth particle hydrodynamics methods with applications in metal forming simulations', *International journal for numerical methods in engineering*, vol. 47, pp. 1189-1214
- [Cleary & Monaghan; 1999] Cleary, W.C., Monaghan, J. J., 1999. 'Conduction Modelling Using Smoothed Particle Hydrodynamics', *Journal of Computational Physics*, vol. 148, pp. 227-264
- [Colagrossi & Landrini; 2003] Colagrossi, A, Landrini, M., 2003. 'Numerical simulation of interfacial flows by smoothed particle hydrodynamics', *Journal of Computational Physics*, vol. 191, pp. 448-475
- [Crespo et. Al; 2007] Crespo. A.J.C., Gómez-Gesteira, M., Dalrymple, R.A., 2007. 'Boundary Conditions Generated by Dynamic Particles in SPH Methods', *Computers, materials and continua*, vol. 5, no. 3, pp. 173-184
- [Dalrymple & Knio; 2001] Dalrymple, R.A., ASCE, F., Knio, O., 2001. 'SPH Modelling of Water Waves', *Coastal Dynamics 01: Proceedings of the 4th Conference on Coastal Dynamics*, Lund, Sweden, June 11-15, pp. 779-787
- [Dalrymple & Rogers; 2006] Dalrymple, R.A., Rogers, B. D., 2006. 'Numerical modelling of water waves with the SPH method', *Coastal Engineering*, vol. 53, pp. 141-147
- [De Vuyst et. al; 2005] De Vuyst, T., Vignjevic, R., Campbell, J. C., 2005. 'Coupling between meshless and finite element methods', *International Journal of Impact Engeneering*, vol. 31, pp. 1054-1064
- [Gesteira & Dalrymple; 2004] Gesteira, M.G., Dalrymple, R. A., 2004. 'Using a Three-dimensional Smoothed Particle Hydrodynamics Method for Wave Impact on a Tall Structure', *Journal of waterway, port, coastal and ocean engineering*, vol. 130, no. 2, pp. 63-69

-
- [Gotoh et. al; 2004] Gotoh, H., Shao, S., Memita, T., 2004. ‘SPH-LES Model for numerical investigation of wave interaction with partially immersed breakwater’, *Coastal Engineering Journal*, vol. 46, no. 1, pp. 39-63
- [Lucy; 1977] Lucy, L.B., 1997. ‘A numerical approach to the testing of the fission hypothesis’, *Astronomical Journal*, vol. 82, no. 12, pp. 1013-1024
- [Monaghan; 1989] Monaghan, J.J., 1989. ‘On the Problem of Penetration in Particle Methods’, *Journal of computational physics*, vol. 82, pp. 1-15
- [Monaghan; 1992] Monaghan, J.J., 1992. ‘Smoothed Particle Hydrodynamics’, *Annual Review of Astronomy & Astrophysics*, vol. 30, pp. 543-574
- [Monaghan; 1994] Monaghan, J.J., 1994. ‘Simulating Free Surface Flows with SPH’, *Journal of computational physics*, vol. 110, pp. 399-406
- [Monaghan; 2000] Monaghan, J.J., 2000. ‘SPH without a Tensile Instability’, *Journal of Computational Physics*, vol. 159, pp. 290-311
- [Monaghan; 2005] Monaghan, J.J., 2005. ‘Smoothed Particle Hydrodynamics’, *Reports on progress in physics*, vol. 68, pp. 1703-1759, Retrieved February 1, 2007, from <http://stacks.iop.org/RoPP/68/1703>
- [Monaghan & Kos; 1999] Monaghan, J.J., Kos, A., 1999. ‘Solitary Waves on a Cretan Beach’, *Journal of waterway, port, coastal and ocean engineering*, vol. 125, pp. 145-154
- [Morris et. al; 1997] Morris, J.P., Fox, P.J., Zhu, Y., 1997. ‘Modelling Low Reynolds Number Incompressible Flows Using SPH’, *Journal of computational physics*, vol. 136, pp. 214-226
- [Shao et. al; 2006] Shao, S., Ji, C., Graham, D.I., Reeve, D.E, James, P.W., Chadwick, A.J., 2006. ‘Simulation of wave overtopping by an incompressible SPH model’, *Coastal Engineering*, vol. 53, pp. 723-735

7.2. Other possible SPH problems

[Violeau & Issa; 2007] Violeau, D., Issa, R., 2007. ‘Numerical modelling of complex turbulent free-surface flows with the SPH method: an overview’, *International Journal for numerical methods in fluids*, vol. 53, pp. 227-304

[Wendland; 1995] Wendland, H., 1995. ‘Piecewise polynomial, positive definite and compactly supported radial functions of minimal degree’, *Advances in Computational Mathematics*, vol. 4, pp. 389-396

Web-sites

[IMSL; 2007] Retrieved January 7, from <http://www.vni.com/products/imsl/documentation/CNL06/stat/NetHelp/default.htm?url=crosscorrelation.htm>

[Farm1; 2007] Retrieved November 1, from http://farm1.static.flickr.com/76/185488383_b48a2c2-dcf.jpg

[Nexlimit; 2007] Retrieved September 9, from <http://www.nextlimit.com/xflow/index.htm>

[Oceanatlas; 2007] Retrieved November 1, from <http://www.oceansatlas.com/unatlas/uses/EnergyResources/Background/Windjte/Image7.jpg>

[ParaView; 2008] Retrieved January 16, from <http://www.paraview.org/New/index.html>

[SPHerics; 2007a] Retrieved August 24, from http://wiki.manchester.ac.uk/spheric/index.php/Main_Page

[SPHerics; 2007b] Retrieved October 24, from http://wiki.manchester.ac.uk/spheric/index.php/Database_of_SPH_literature

[SPHysics; 2007] Retrieved October 24, from http://wiki.manchester.ac.uk/sphysics/index.php/Main_Page

[Wave dragon; 2008] Retrieved February 4, from <http://www.offshorecenter.dk/log/filer/WD.jpg>

[Wave star; 2008] Retrieved February 4, from <http://www.folkecenter.net/mediafiles/folkecenter/rd/wave/WaveStarEnergy.jpg>

[WaveLab2; 2007] Retrieved December 8, from <http://hydrosoft.civil.aau.dk/wavelab/>

[Rogers; 2008] Retrieved January 20, from http://www.ce.jhu.edu/brogers/research/SPH_Open_Boundaries.html

Other

[Gesteira et. al; 2007] Gesteira, M.G., Rogers, B.D, Dalrymple, R.A., Crespo, A. J. C., Narayanaswamy, M, 2007. *User guide for the SPHysics code*, Retrieved October 24, 2007, from http://wiki.manchester.ac.uk/sphysics/images/SPHysics_GUIDE.pdf